Accepted Manuscript

Novel cationic Bis(acylhydrazones) as modulators of Epstein–Barr virus immune evasion acting through disruption of interaction between nucleolin and G-quadruplexes of EBNA1 mRNA

Oksana Reznichenko, Alicia Quillévéré, Rodrigo Prado Martins, Nadège Loaëc, Hang Kang, María José Lista, Claire Beauvineau, Jorge González-García, Régis Guillot, Cécile Voisset, Chrysoula Daskalogianni, Robin Fåhraeus, Marie-Paule Teulade-Fichou, Marc Blondel, Anton Granzhan

PII: S0223-5234(19)30452-0

DOI: https://doi.org/10.1016/j.ejmech.2019.05.042

Reference: EJMECH 11352

To appear in: *European Journal of Medicinal Chemistry*

Received Date: 21 February 2019

Revised Date: 25 April 2019

Accepted Date: 15 May 2019

Please cite this article as: O. Reznichenko, A. Quillévéré, R.P. Martins, Nadè. Loaëc, H. Kang, Marí.José. Lista, C. Beauvineau, J. González-García, Ré. Guillot, Cé. Voisset, C. Daskalogianni, R. Fåhraeus, M.-P. Teulade-Fichou, M. Blondel, A. Granzhan, Novel cationic Bis(acylhydrazones) as modulators of Epstein–Barr virus immune evasion acting through disruption of interaction between nucleolin and G-quadruplexes of EBNA1 mRNA, *European Journal of Medicinal Chemistry* (2019), doi: https://doi.org/10.1016/j.ejmech.2019.05.042.

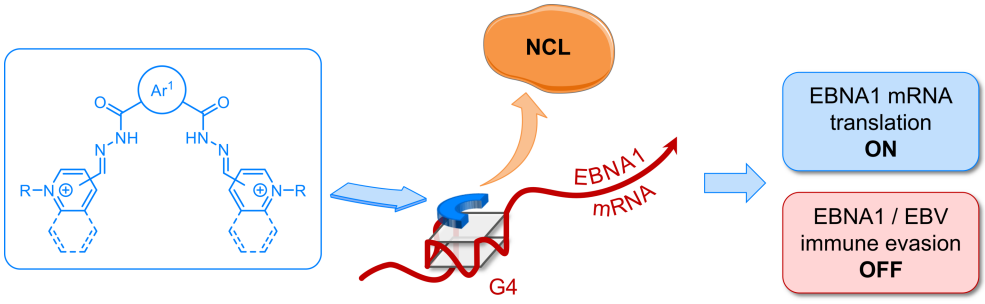

Novel Cationic Bis(acylhydrazones) as Modulators of Epstein–Barr Virus Immune Evasion Acting through Disruption of Interaction between Nucleolin and G-quadruplexes of EBNA1 mRNA

Oksana Reznichenko,[a,b,1] Alicia Quillévéré,[c,1] Rodrigo Prado Martins,[d,1] Nadège Loaëc,[c] Hang Kang,[a,b] María José Lista,[c] Claire Beauvineau,[a,b] Jorge González-García,[a,b] Régis Guillot,[e] Cécile Voisset,[c] Chrysoula Daskalogianni,[d] Robin Fåhraeus,[d] Marie-Paule Teulade-Fichou,[a,b,*] Marc Blondel,[c,2,*] Anton Granzhan[a,b,2,*]

[a] *CNRS UMR9187, INSERM U1196, Institut Curie, PSL Research University, 91405 Orsay, France*

[b] *CNRS UMR9187, INSERM U1196, Université Paris Sud, Université Paris-Saclay, 91405 Orsay, France*

[c] *INSERM UMR1078, Université de Bretagne Occidentale (UBO), Établissement Français du Sang (EFS) Bretagne, CHRU Brest, 29200 Brest, France*

[d] *INSERM UMR1131, Institut de Génétique Moléculaire (IGM), Université Paris 7, Hôpital St. Louis, 75010 Paris, France*

[e] *CNRS UMR8182, Institut de Chimie Moléculaire et des Matériaux d'Orsay (ICMMO), Université Paris Sud, Université Paris-Saclay, 91405 Orsay, France*

[1,2] *Equal contribution.*

** Corresponding authors. E-mail addresses: mp.teulade-fichou@curie.fr (MPTF), marc.blondel@univ-brest.fr (MB), anton.granzhan@curie.fr (AG).*

HIGHLIGHTS

- Interaction of NCL with G4 of EBNA1 mRNA is involved into immune evasion of EBNA1 and EBV
- Cationic bis(acylhydrazones) were developed as novel ligands binding to G4 of EBNA1 mRNA
- SAR of novel ligands with respect to *in vitro* binding to G4 of EBNA1 mRNA is discussed
- Two novel ligands enhance the expression of EBNA1 and antigen presentation
- Novel ligands disrupt the NCL–EBNA1 mRNA interaction *in cellulo* as shown by PLA

ABSTRACT

The oncogenic Epstein–Barr virus (EBV) evades the immune system through limiting the expression of its highly antigenic and essential genome maintenance protein, EBNA1, to the minimal level to ensure viral genome replication, thereby also minimizing the production of EBNA1-derived antigenic peptides. This regulation is based on inhibition of translation of the virally-encoded EBNA1 mRNA, and involves the interaction of host protein nucleolin (NCL) with G-quadruplex (G4) structures that form in the glycine–alanine repeat (GAr)-encoding sequence of the EBNA1 mRNA. Ligands that bind to these G4-RNA can prevent their interaction with NCL, leading to disinhibition of EBNA1 expression and antigen presentation, thereby interfering with the immune evasion of EBNA1 and therefore of EBV (M. Lista et al., *Nature Commun*., **2017**, *8*, 16043). In this work, we synthesized and studied a series of 20 cationic bis(acylhydrazone) derivatives designed as G4 ligands. The *in vitro* evaluation showed that most derivatives based on central pyridine (Py), naphthyridine (Naph) or phenanthroline (Phen) units were efficient G4 binders, in contrast to their pyrimidine (Pym) counterparts, which were poor G4 binders due a significantly different molecular geometry. The influence of lateral heterocyclic units (*N*-substituted pyridinium or quinolinium residues) on G4-binding properties was also investigated. Two novel compounds, namely **PyDH2** and **PhenDH2**, when used at a 5 µM concentration, were able to significantly enhance EBNA1 expression in H1299 cells in a GAr-dependent manner, while being significantly less toxic than the prototype drug **PhenDC3** (GI_{50} > 50 µM). Antigen presentation, RNA pull-down and proximity ligation assays confirmed that the effect of both drugs was related to the disruption of NCL–EBNA1 mRNA interaction and the subsequent promotion of GAr-restricted antigen presentation. Our work provides a novel modular scaffold for the development of G-quadruplex-targeting drugs acting through interference with G4-protein interaction.

KEYWORDS

Epstein–Barr virus • G-quadruplex RNA • G-quadruplex ligands • Nucleolin • Immune evasion

1. INTRODUCTION

The Epstein–Barr virus (EBV) is the first oncogenic virus discovered in human. Most of world's adult population (>90%) is infected with the virus but do not develop any pathology [1]. However, a small proportion of infected individuals develops EBV-linked cancers, which include Burkitt and Hodgkin lymphomas, and up to 10% gastric carcinomas, as well as nasopharyngeal carcinoma, particularly frequent among men in China and Tunisia [1,2]. Like all gamma-herpesviruses, EBV effectively evades the host immune system but has an Achilles heel, namely its genome maintenance protein EBNA1. EBNA1 is essential for EBV genome replication and maintenance and, as such, is expressed in all dividing EBV-infected cells. On the other hand, EBNA1 is highly antigenic, and $CD8^+$ T cells directed towards EBNA1 epitopes are present in all infected individuals. Hence, EBV has seemingly evolved a mechanism to limit EBNA1 production to the minimal level required for the viral genome replication thereby, at the same time, minimizing the production of EBNA1-derived antigenic peptides presented to the cytotoxic T cells through the major histocompatibility complex (MHC) class I pathway. The central glycine–alanine repeat (GAr) of EBNA1 plays a critical role in this mechanism of immune evasion, as it is able to self-inhibit the translation of its own mRNA *in cis*. Remarkably, infection by an EBV strain encoding a truncated version of EBNA1 in which GAr has been deleted (EBNA1ΔGAr) leads to high level of EBNA1 protein and to an efficient T cell response, which demonstrates the critical role of GAr in EBNA1 immune evasion [3]. GAr-based EBNA1 immune evasion is considered a relevant therapeutic target in the treatment of EBV-related cancers, since most tumor cells from these cancers are infected by EBV whereas, in healthy individuals, the latent infection by EBV is primarily restricted to a specific small pool of memory B cells. Hence, overcoming the GAr-based self-inhibition of EBNA1 translation should unveil EBV-carrying tumor cells to cytotoxic T cells without having significant effect on the vast majority of healthy host cells. Of note, GAr is polymorphic with respect to its length and, importantly, the effect of GAr is length-dependent: longer domains display a stronger inhibitory effect on both mRNA translation and antigen presentation [4–6].

The GAr-encoding mRNA sequence is GC-rich and is capable of forming multiple G-quadruplex (G4) structures, which were shown to be implicated in the regulation of EBNA1 synthesis *in vitro* [7]. G4s are particular secondary structures of nucleic acids formed through the stacking of G-quartets, that is, planar arrangements of four guanines connected by Hoogsteen hydrogen bonds. G4 structures within G-rich DNA or RNA sequences have been implicated in gene regulation where they can affect transcription, splicing and translation [8,9]. The mechanisms of G4-based regulation are still poorly understood, but cellular factors that interact with these structures are rapidly emerging [10,11]. Moreover, an increasing number of pathologies, that include cancer, neurodegenerative disorders,

bacterial and viral diseases, have been associated with G4-based regulation, illustrating the potential importance of these structures as therapeutic targets [12–17].

Along these lines, we have previously developed a yeast (*Saccharomyces cerevisiae*)-based assay reproducing all the aspects of the GAr-based inhibition of translation, including the GAr-length dependency [18]. This allowed us to decipher the mechanisms of GAr-mediated mRNA translation suppression *in cis* and, in particular, to identify the cellular factors involved [19,20]. The yeast assay was successfully used first to identify small molecular-weight compounds that can stimulate EBNA1 expression both in yeast and in mammalian cells and relieve the GAr-based limitation of antigen presentation [18,20]. More recently, this model was employed for a genetic screen that aimed at identifying host cell genes involved in the GAr-mediated inhibition of translation. This enabled us to identify the yeast *NSR1* gene encoding the ortholog of human nucleolin (NCL) [21], and to demonstrate that NCL is critically involved in the GAr-based limitation of EBNA1 translation and antigen presentation, and thus in the immune evasion of EBV. Specifically, we showed that NCL directly interacts in the nucleus (or in close vicinity of the nucleus) with G4s that form in the GAr-encoding sequence of EBNA1 mRNA and inhibits its translation, thereby limiting the production of EBNA1-derived antigenic peptides which, in turn, favors immune evasion of EBV-infected cells [22]. Consequently, the interaction of NCL with G4 of EBNA1 mRNA appears a relevant therapeutic target for the treatment and/or prevention of EBV-related cancers, as drugs that disrupt this interaction could, in principle, overcome the GAr-based EBNA1 immune evasion of EBV. In line, we demonstrated that the benchmark G4 ligand **PhenDC3** is able to prevent NCL from binding to G4s formed in the GAr mRNA sequence, and to stimulate GAr-limited translation and antigen presentation (Fig. 1a) [22]. Importantly, this ability of **PhenDC3** is not a general property of all the G4-ligands since the other benchmark G4 ligand, pyridostatine (**PDS**), has no effect on NCL binding nor on GAr-based inhibition of translation. Hence, it appears that active G4 ligands not only need to bind efficiently to G4 that form in the GAr-encoding sequence of EBNA1 mRNA, but they should also be able to interfere with NCL binding, which does not appear as a general property of all G4 ligands.

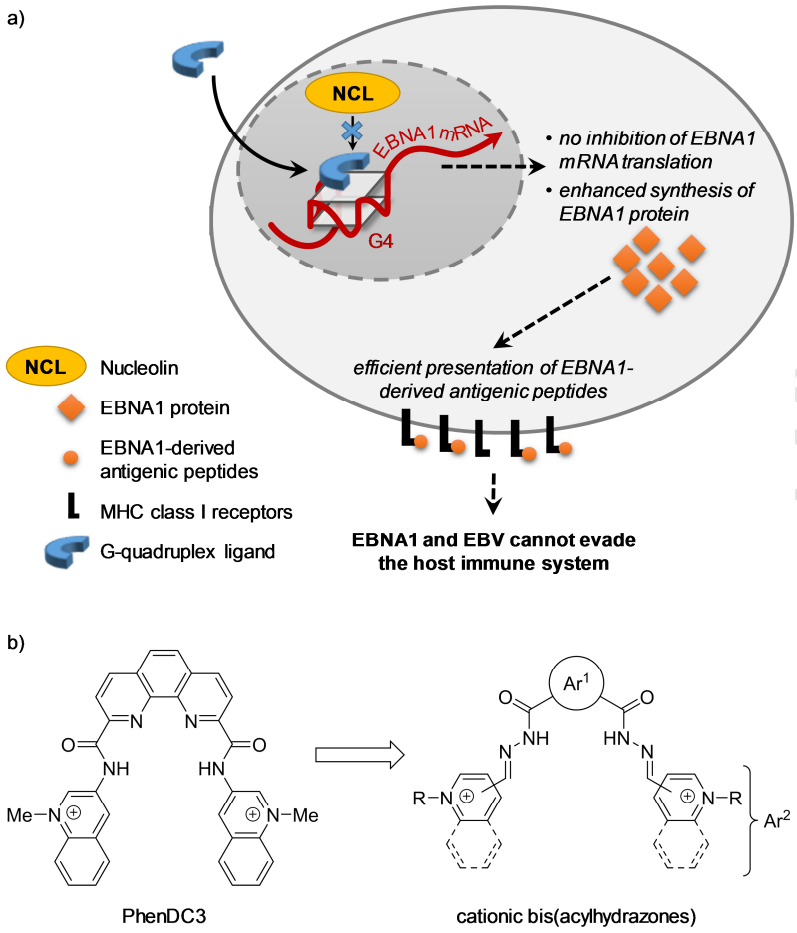

Fig. 1. a) Effect of G-quadruplex ligands on the nucleolin (NCL)- and GAr-dependent limitation of EBNA1 synthesis. NCL binds directly to G-quadruplexes (G4s) formed in the GAr-encoding sequence of EBNA1 mRNA, thus inhibiting its translation and thereby leading to a weak production of EBNA1 protein and EBNA1-derived antigenic peptides. This allows EBNA1 and EBV to evade the immune system. Some G4 ligands like **PhenDC3** compete with NCL for binding to G4s of EBNA1 mRNA, thereby relieving the inhibitory effect of GAr and NCL on both translation and antigen presentation. b) Design of cationic bis(acylhydrazone) ligands featuring shape similarity to **PhenDC3**.

With the aim to explore new pharmaceutical scaffolds as putative G4 ligands and disruptors of the NCL–EBNA1 G4-mRNA interactions, we designed a series of cationic bis(acylhydrazone) derivatives representing shape analogues of **PhenDC3** (Fig. 1b). These U-shaped scaffolds are expected to provide an optimal overlap with G-tetrads, as demonstrated by the structural model of **PhenDC3** bound to a parallel-stranded G4-DNA substrate [23]. In addition, the *N*-acylhydrazone group has been identified as a privileged scaffold in drug design, due to a combination of hydrogen-bond acceptor and donor sites capable of interactions with a wide range of biomolecules. Despite the fact that acylhydrazone derivatives are rapidly metabolized, this motif is encountered in several approved drugs (e.g., nifuroxazide and dantrolene) [24] and drug candidates [25–27]. The facile synthetic availability of acylhydrazone derivatives, which allows furnishing congeneric series of compounds

with distinct physico-chemical properties and bioactivities, makes it a promising scaffold in the drug discovery field [28–30]. Herein, we describe the synthesis of novel derivatives and the determination of their *in vitro* and *in cellulo* ability to bind to G4 of EBNA1 mRNA, as well as their effect on NCL-mediated GAr-dependent limitation of EBNA1 expression and antigen presentation.

2. RESULTS

2.1. Chemistry

The design of cationic bis(acylhydrazones) features a central heterocyclic core Ar^1, i.e., a derivative of pyridine (Py), pyrimidine (Pym), 1,8-naphthyridine (Naph), or 1,10-phenanthroline (Phen), connected via two acyhydrazone linkages to lateral, *N*-substituted cationic heterocycles (Ar^2 = pyridinium or quinolinium, R = Me, Et, or Bn). Our initial approach to the synthesis of these derivatives relied on the formation of neutral bis(acylhydrazone) precursors, followed by quaternization of lateral heterocyclic residues (Scheme 1, path A). Thus, four heterocyclic bis(acylhydrazides) **1–4**, obtained by a hydrazinolysis of the corresponding dimethyl esters, were made to react with three heteroaromatic aldehydes **5a–c**, to give the 11 corresponding bis(acylhydrazones) **6a–c**, **7a–c**, **8a–c** and **9a–c**, with yields ranging from 55 to 99% (Experimental Part). Subsequent quaternization using excess alkyl or benzyl halide gave the corresponding cationic bis(acylhydrazones). However, while some products (e.g., **PyDH1**, **PyDH2**) could be obtained in a pure form after a single recrystallization, several other ones (e.g., **PymDH1**, **PymDH2**, **NaphDH2**) contained up to 20% (as per ^{1}H NMR) of mono-alkylated product as an impurity, which could not be removed even after repeated recrystallizations. Therefore, we elaborated an alternative synthesis of these derivatives (Scheme 1, path B), relying on *N*-alkylation of heteroaromatic aldehydes in a first step, and obtained five quaternized aldehydes (**10a**, **11a–b**, **12a–b**) isolated as stable, but hygroscopic salts in good yields (73–94%). The subsequent condensation of the latter with bis(acylhydrazides) **1–4** gave a series of 20 cationic bis(acyl-hydrazones) (**PyDH1–5**, **PymDH1–5**, **NaphDH1–5**, and **PhenDH1–5**, Table 1), all obtained as iodide or bromide salts in good yields (50–97%) and excellent purity after a single recrystallization. The identity and purity of all final compounds were confirmed using spectroscopic and chromatographic methods and combustion analysis.

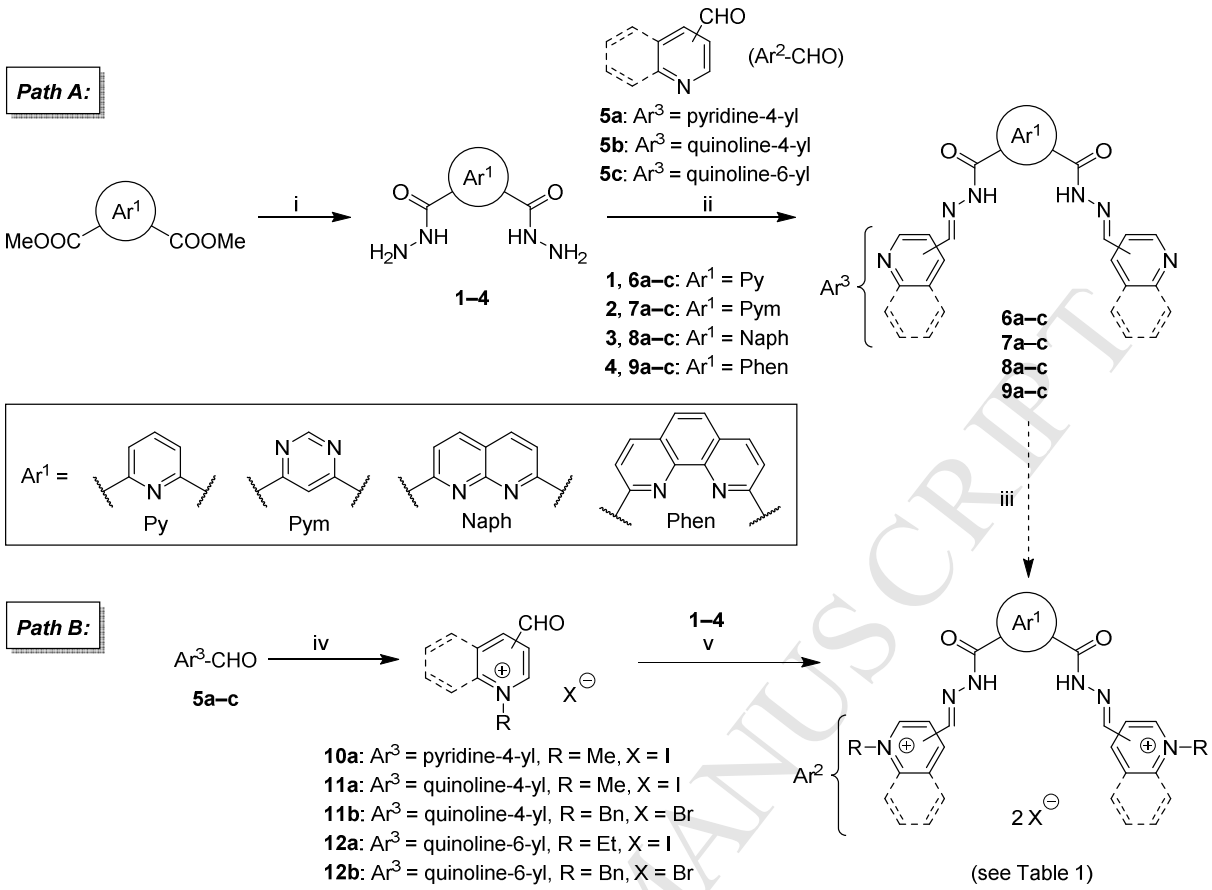

Scheme 1. Synthesis of cationic bis(acylhydrazones). Reagents and conditions: (i) $N_2H_4 \times H_2O$, EtOH, reflux, 18 h; (ii) EtOH, reflux, 18 h; (iii) RX, DMF, 40 °C or 60 °C, 18 h; (iv) RX, DCM, r.t., 72 h or acetone, reflux, 18 h; (v) DMF, 80 °C or 100 °C, 2 h.

Table 1. Structures of novel cationic bis(acylhydrazones)

Ar^1 \ Ar^2	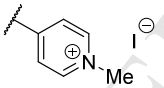	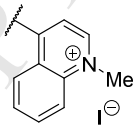	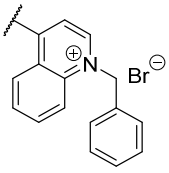	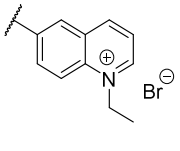	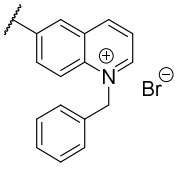
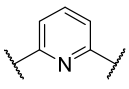	**PyDH1**	**PyDH2**	**PyDH3**	**PyDH4**	**PyDH5**
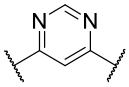	**PymDH1**	**PymDH2**	**PymDH3**	**PymDH4**	**PymDH5**
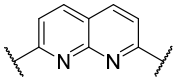	**NaphDH1**	**NaphDH2**	**NaphDH3**	**NaphDH4**	**NaphDH5**
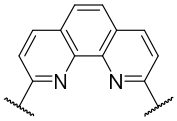	**PhenDH1**	**PhenDH2**	**PhenDH3**	**PhenDH4**	**PhenDH5**

2.2. Structural characterization

X-ray quality crystals of **PyDH1** ($2I^-$), **PymDH1** ($2I^-$), and **PhenDH1** ($2I^-$) could be obtained from acetonitrile–water (in the case of **PymDH1** ($2I^-$), a simultaneous formation of yellow and orange polymorphs was observed, both belonging to the $\overline{P1}$ space group but differing by the packing of cations). Single-crystal diffraction analysis revealed that in all three compounds the organic cations were essentially planar, with minimal twisting at the level of terminal heterocyclic rings breaking the two-fold molecular symmetry (Fig. 2). In all cases, both *N*-acylhydrazone groups adopted *E*–*antiperiplanar* conformation. Remarkably, **PyDH1** and **PhenDH1** revealed co-crystallized water molecules located in between the two acylhydrazone groups and forming hydrogen bonds with both amide NH groups (**PyDH1**: *d*(NH···O) = 2.84 and 2.90 Å, *α*(N-H···O) = 150°; **PhenDH1**: *d*(NH···O) = 2.85 and 2.84 Å, *α*(N-H···O) ≈ 170°). In addition, in **PyDH1** the water molecule formed a weak hydrogen bond with the pyridine nitrogen (*d*(N···O) = 3.08 Å, Fig. 2, a), whereas in **PhenDH1** it formed a stronger, bifurcated hydrogen bonds with both phenanthroline nitrogens (mean *d*(N···O) = 2.95 Å, Fig. 2c). The coordination of water molecules thus determines the inward-folded, V-shaped conformation of **PyDH1**, similar to what was observed with related, charge-neutral pyridine-2,6-bis(acylhydrazones) [31], as well as the U-shaped conformation of **PhenDH1** which is further stabilized due to the number and favorable arrangement of hydrogen bonds. In contrast, **PymDH1** (Fig. 2b) was found to adopt a linear conformation, partially stabilized by intramolecular bonds between the amide NH groups and nitrogen atoms of the pyrimidine core (*d*(N···N) = 2.66 Å). Although this compound also crystallized along with water molecules, the latter were found to coordinate to amide CO groups, on one hand, and iodide anions, on the other hand (not shown).

It may be suggested that the described interactions with water molecules persist in aqueous solutions, governing the molecular shape of bis(acylhydrazone) ligands. In this context, V- or U-shaped derivatives **PyDH*n*** and **PhenDH*n***, presumably, have a more favorable structure for binding to G4-quadruplex structures due to a more complete overlap with G-tetrads, as compared to linear analogues **PymDH*n***.

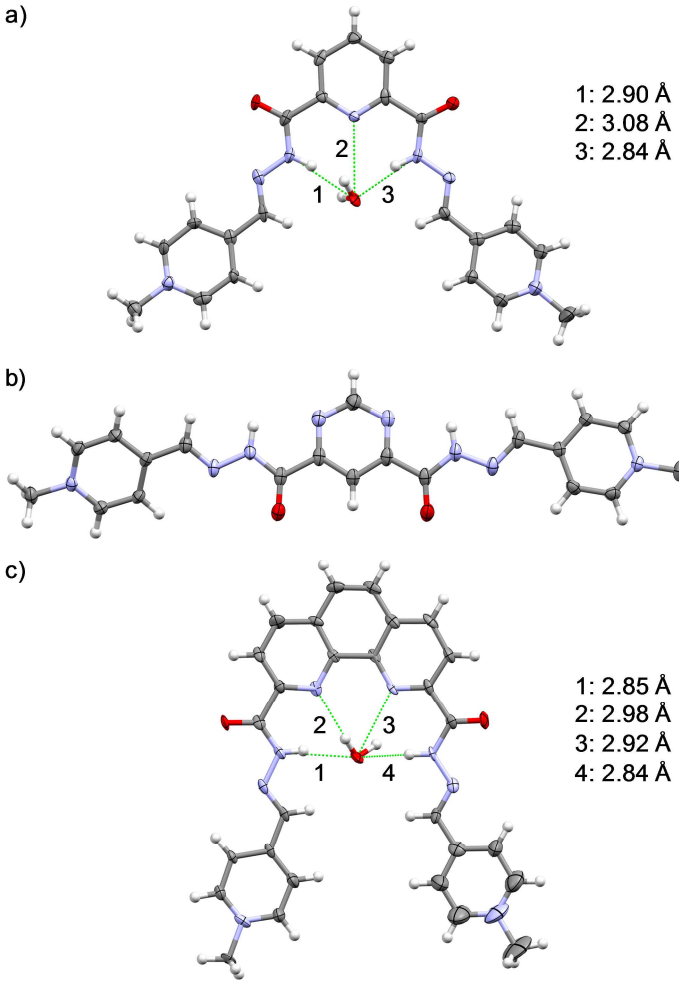

Fig. 2. Solid-state structures of a) **PyDH1** ($2I^-$) × 2 H_2O, b) **PymDH1** ($2I^-$) × 2 H_2O × MeCN (yellow form), and c) **PhenDH1** ($2I^-$) × 2 H_2O × MeCN, from single-crystal X-ray diffraction analysis. Non-bound water, acetonitrile molecules and counter-ions were omitted for clarity. CPK atom colors; green lines and labels indicate intermolecular hydrogen bonds with crystallized water molecules and the corresponding N···O distances.

2.3. *In silico* evaluation

The drug-like properties of cationic bis(acylhydrazones) were evaluated using SwissADME, a free tool allowing to assess the physicochemical descriptors, pharmacokinetics (ADME), and drug-likeness of small molecules [32]. It should be noted that certain methods of *in silico* evaluation are poorly suitable for cationic compounds as the ones described in this work, as illustrated by significant variance of physico-chemical properties predicted by different algorithms for the same compound (e.g. for **PyDH1**, cLogP from –7.75 to 1.83, Table S1). According to the established practices, consensus estimation (i.e., the average of five models) was used in evaluation of drug-likeness of compounds [32]. The results of *in silico* assessment (Fig. S1 and Table S1) indicated satisfactory bioavailability for most bis(acylhydrazones), as given by the combination of six physicochemical descriptors (lipophilicity, molecular weight, polarity, solubility, saturation and number of rotatable bonds). Among those, insufficient saturation (i.e., low fraction of sp^3 carbons) could be identified as

the limiting factor for bioavailability of most derivatives, as well as high molecular weight for the derivatives **NaphDH3**, **NaphDH5**, **PhenDH3** and **PhenDH5** (*M* > 700 Da). With the exception of the latter four derivatives, all bis(acylhydrazones) satisfied the Lipinski's rule, and most derivatives also satisfied the Muegge's rule [33], indicating a high potential to serve as drugs (Table S1). Finally, we employed a gastrointestinal absorption predictor calculated by the BOILED-egg model (Fig. 3) [34]. According to this model, most compounds, again with the exception of **NaphDH3**, **NaphDH5**, and **PhenDH3–5**, had a high rate of passive gastrointestinal absorption; however, none of compounds was expected to cross the blood-brain barrier (Fig. 3). In conclusion, the results of *in silico* evaluation indicate that the cationic bis(acylhydrazone) scaffolds are compatible with their use as RNA-targeting drugs, while heavy and aromatic substitutes (e.g., R = Bn) should be avoided for the sake of bioavailability, unless indispensable for RNA binding.

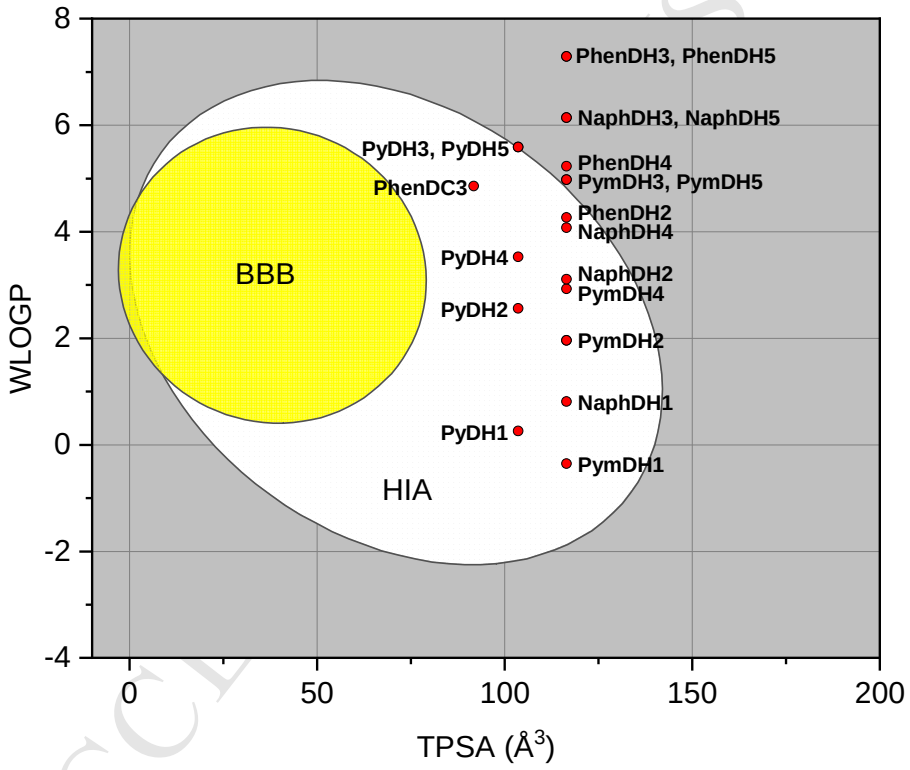

Fig. 3. BOILED-egg evaluation [34] of passive gastrointestinal absorption (HIA) and brain (BBB) penetration of bis(acylhydrazones). The white region indicates high probability of passive gastrointestinal absorption, and the yellow region indicates high probability of BBB penetration.

The compounds were also assessed for the presence of fragments associated with pan-assay interfering compounds (PAINS). The presence of quinolinium fragments was identified as potentially troublesome in some (but not all) compounds (Table S1); however, an inspection of the original screen revealed that this fragment was mainly associated with cationic dyes, potentially interfering with colorimetric or fluorimetric assays [35]. Since bis(acyhydrazones) are colorless or faintly colored

compounds, this filter was not applied and all compounds were systematically assessed by biophysical and biological tests.

2.4. Biophysical studies of interaction of novel ligands with G4 of EBNA1 mRNA and G4-DNA

The interaction of novel bis(acylhydrazone) derivatives with the most frequent G4-forming motif encountered in GAr-encoding sequence of the EBNA1 mRNA (g4-EBNA1, 5′-r(**GGGG**CA**GG**A-GCA**GG**A**GG**A)-3′) was studied *in vitro* using two widely established methods, namely fluorescence-monitored thermal denaturation (fluorescence melting) and fluorescent indicator displacement (FID) assay. In the first method, the binding of ligands is manifested by an increase of denaturation temperature (ΔT_m) of oligoribonucleotide F-g4-EBNA1-T, bearing a fluorophore (5′, 6-FAM) and a quencher (3′, TAMRA). In our conditions (10 mM $KAsO_2Me_2$, 10 mM KCl, 90 mM LiCl buffer, pH 7.3) and in the absence of ligands, F-g4-EBNA1-T denatured at T_m^0 = 58.6 °C, which is slightly higher than the reported value (54 °C) [7]. In addition to the ranking of ligands with respect to their ability to stabilize the G4 substrate, fluorescence melting experiments provide information on G4-RNA vs. ds-DNA selectivity of ligands, namely through analysis of the drop of ΔT_m values observed in the presence of unlabeled, double-stranded DNA competitor (ds26, 15 or 50 molar equivalents) [36]. The results (Fig. 4, a) demonstrate that bis(acylhydrazone) derivatives display great variability with respect to their capacity to bind to and stabilize g4-EBNA1, revealing interesting structure–activity relationships discussed in details below. Specifically, most derivatives of the PyDH and NaphDH families, as well as PhenDH1, demonstrated significant stabilization of g4-EBNA1 (ΔT_m = 10 to 20 °C), and further phenanthroline derivatives (**PhenDH2–5**) demonstrated even higher stabilization of the substrate (ΔT_m = 20 to 30 °C), comparable to the result obtained with **PhenDC3** (ΔT_m = 30.0 °C). In contrast, all derivatives of the PymDH family, as well as compounds **PyDH1** and **NaphDH1**, demonstrated low or very low stabilization of G4-RNA (ΔT_m < 10 °C), illustrating the importance of the nature of heterocyclic residues on the G4-RNA binding properties of ligands. Finally, most derivatives that stabilized g4-EBNA1 also displayed significant level of selectivity with respect to ds-DNA, as their stabilizing effect was almost unaffected by the presence of ds-DNA competitor.

To assess the selectivity of novel ligands for G4 of EBNA1 mRNA, additional fluorescence melting experiments were performed with two G4-DNA substrates, namely F-24TTG-T (predominantly a hybrid-1 G4 structure, adopted by a variant of human telomeric DNA sequence) [37] and F-myc22-T (parallel-stranded G4-DNA, adopted by variant of the G4-forming sequence from the promoter region of *c-Myc* oncogene) [38]. The results (Fig. S2) demonstrate no preferential stabilization of one or another substrate, since all compounds that stabilized g4-EBNA1 (**PyDH2–5**, **NaphDH2–5**, and all PhenDH derivatives) also strongly stabilized both G4-DNA substrates (with ΔT_m = 15 to 30 °C). A similar behavior was observed with PhenDC3, which stabilized both G4-DNA with ΔT_m of over 35 °C.

The lack of selectivity is not surprising given the structural similarity of novel ligands to **PhenDC3** (a polyvalent G4 binder) and indicates a similar binding mode, relying on compound stacking with terminal G-tetrads of G4 structures. Obviously, the substituents explored in this work (ethyl or phenyl groups) are not sufficient for achieving a significant level of selectivity between different G4 structures.

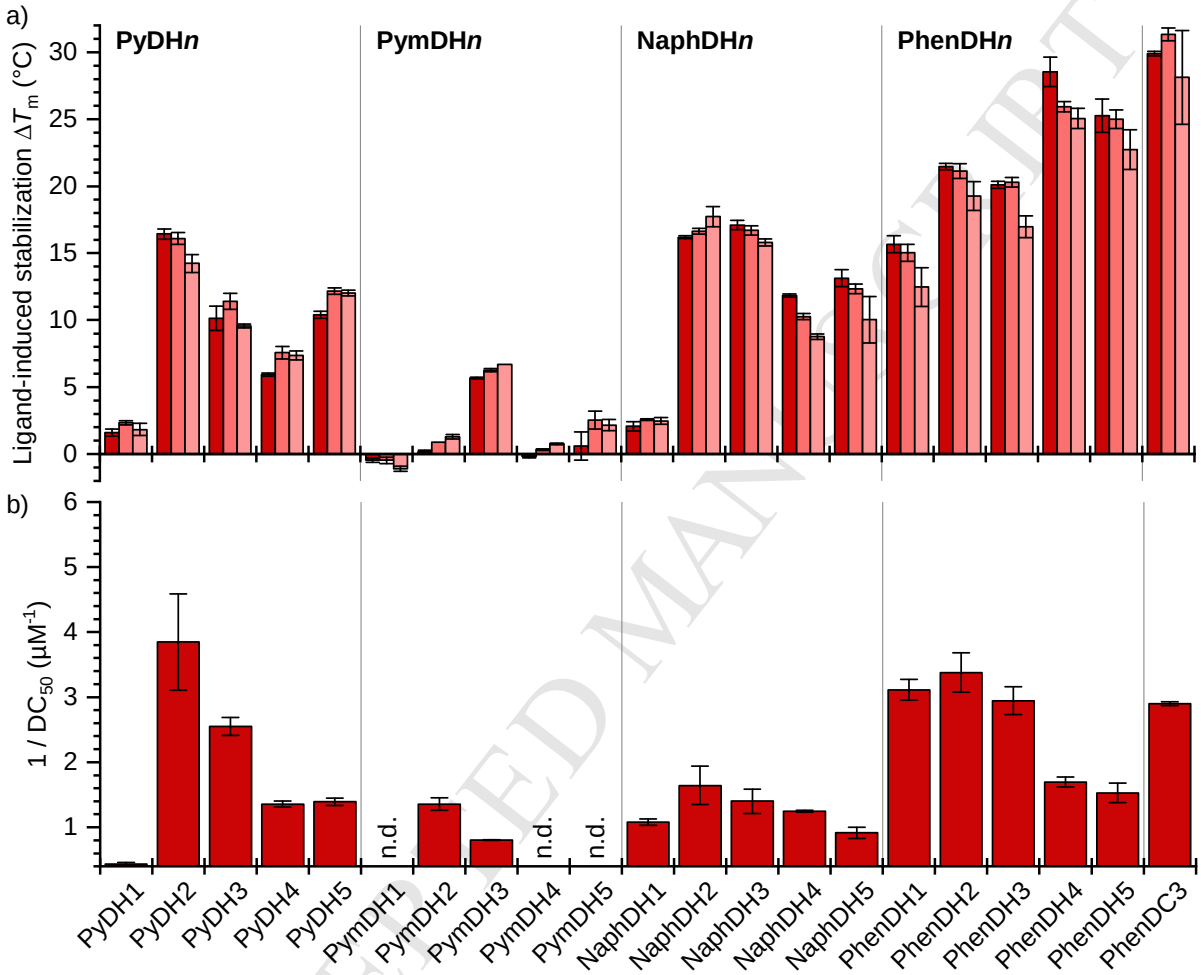

Fig. 4. *In vitro* binding of tested compounds to g4-EBNA1. a) Thermal stabilization F-g4-EBNA1-T (0.2 μM) by tested compounds (1.0 μM), assessed by fluorescence melting experiments in the absence (dark red bars) or in the presence of duplex DNA competitor ds26 (red bards: 3 μM, pale red bars: 10 μM). The experiments were performed in K10 buffer (10 mM $LiAsO_2Me_2$, 10 mM KCl, 90 mM LiCl, pH 7.3); data are means ± s.d. from three technical replicates. b) Ligand-induced displacement of TO (0.5 μM) from g4-EBNA1 (0.25 μM). Data are means ± s.d. from three technical replicates; n.d. = no displacement (DC_{50} > 2.5 μM). The experiments were performed in K100 buffer (10 mM $LiAsO_2Me_2$, 100 mM KCl, 1 mM EDTA, 1% v/v DMSO).

A complementary information about ligand affinity for g4-EBNA1 was obtained from the FID assay, which assesses the binding of ligands through displacement of a fluorescent probe (Thiazole Orange, TO). In this assay, the apparent ligand affinity is given by the concentration required to displace 50% of the bound probe (DC_{50}) [39]. The results of the FID assay (Fig. 4b and Table S2) indicated high g4-

EBNA1 affinity (DC_{50} < 0.5 μM) for compounds **PyDH2**, **PyDH3**, as well as **PhenDH1–3**, which was comparable to the result obtained for **PhenDC3** (DC_{50} = 0.31 μM). In contrast, the derivatives **PyDH1**, **PymDH1**, **PymDH4** and **PyDH5** were not able to displace TO from g4-EBNA1 (DC_{50} > 2 μM), giving evidence of low affinity, whereas other derivatives demonstrated moderate affinity (DC_{50} = 0.5 to 2 μM). Of note, none of tested ligands was able to induce displacement of TO from the double-stranded DNA substrate ds26 (DC_{50} > 2.5 μM in all cases). Globally, the results obtained with both biophysical methods were in a good agreement, except for a few discrepancies (compounds **PyDH5**, **NaphDH2–5** and **PhenDH4–5** which demonstrated high thermal stabilization of g4-EBNA but only moderate capacity to displace TO, DC_{50} = 0.5 to 1 μM). Altogether, the results of biophysical studies point to pyridine derivatives **PyDH2** and **PyDH3**, as well as all derivatives of the phenanthroline series, as most promising ligands for g4-EBNA.

2.5. Biological tests

2.5.1. Effect of compounds on GAr-dependent protein expression

To assay the biological activity of the various compounds bis(acylhydrazones), we first determined their effect on the GAr-dependent limitation of EBNA1 expression, which represents a mechanism at the basis of EBNA1/EBV immune evasion. For this purpose, human lung carcinoma H1299 cells were transfected with EBNA1 or EBNA1ΔGAr constructs and treated with 10 μM of the indicated compounds or, as a control, with DMSO (the vehicle). Then, the levels of EBNA1 or EBNA1ΔGAr was assessed by western blot analysis using an antibody raised against EBNA1 and, as a loading control, an antibody raised against GAPDH. **PhenDC3** was used as a positive control and DMSO as a negative control. In this assay, three types of results were observed (Table 2): (i) most of the compounds had no effect (indicated by a "0"); (ii) two compounds, namely **PyDH2** and **PhenDH2**, similarly to **PhenDC3**, led to a GAr-dependent increase in EBNA1 expression, indicated by a "+" (i.e., they increased EBNA1 level while having no effect on EBNA1ΔGAr); and finally (iii) three compounds (**PyDH3**, **PymDH5**, and **PhenDH1**) increased EBNA1 level in a GAr-independent manner indicated by a "×" (i.e., they increased both EBNA1 and EBNA1ΔGAr levels). The western blot results obtained with compounds **PyDH2** and **PhenDH2** are presented on Fig. 5a. As we were interested in compounds able to interfere with the GAr-dependent limitation of EBNA1 expression and antigen presentation, a mechanism at the basis of EBNA1 immune evasion, we focused only on the compounds that increase EBNA1 level while having no effect on EBNA1ΔGAr, namely **PhenDH2** and **PyDH2**.

Table 2. Effect of compounds (all tested at 5 μM) on EBNA1 expression in H1299 cells.

Compound	Effect[a]	Compound	Effect[a]	Compound	Effect[a]	Compound	Effect[a]
PyDH1	0 (106/93)[b]	**PymDH1**	0 (80/92)[b]	**NaphDH1**	0 (112/99)[b]	**PhenDH1**	× *(78/76)*[b,c]

PyDH2	+ (162/101)[b]	**PymDH2**	0 (89/103)[b]	**NaphDH2**	0 (95/100)[b]	**PhenDH2**	+ (189/96)[b]
PyDH3	× (134/149)[b]	**PymDH3**	0 (108/106)[b]	**NaphDH3**	0 (106/93)[b]	**PhenDH3**	0 (96/114)[b]
PyDH4	0 (86/98)[b]	**PymDH4**	× *(48/47)*[b,c]	**NaphDH4**	0 (82/111)[b]	**PhenDH4**	0 (80/96)[b]
PyDH5	× *(58/70)*[b,c]	PymDH5	×(139/137)[b]	**NaphDH5**	0 (104/108)[b]	**PhenDH5**	0 (111/94)[b]

[a] 0: No effect ; +: GAr-dependent increase in EBNA1 expression; ×: GAr-independent effect. [b] Number between brackets indicate the quantification of respectively GAr-OVA (numerator) and OVA (denominator) levels, as compared to their respective levels in DMSO-treated cells. [c] Values in italics, which are significantly smaller than 100, point to compounds that are toxic to both GAr-OVA- and OVA-expressing cells.

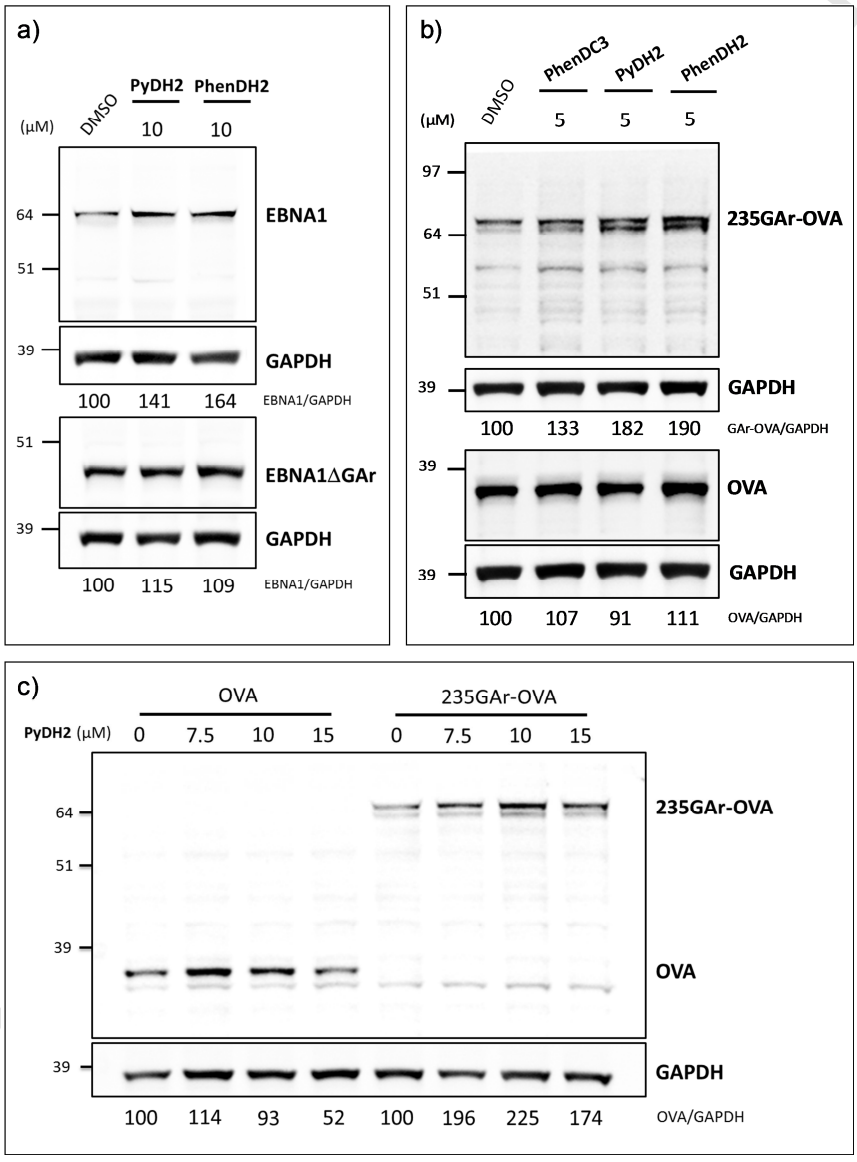

Fig. 5. a) Expression of EBNA1 (top panel) or EBNA1ΔGAr (bottom panel) in transfected H1299 cells treated with DMSO (control), **PyDH2** (10 μM), or **PhenDH2** (10 μM) 40 h post-transfection. b) Expression of 235GAr-OVA (top panel) or OVA (bottom panel) in transfected H1299 cells treated with DMSO (control), **PhenDC3**, **PyDH2**, or **PhenDH2** (all at 10 μM) 40 h post-transfection. c) Expression of 235GAr-OVA or OVA in transfected H1299 cells treated with **PyDH2** used at 0 (control), 7.5, 10, or 15 μM concentration. Protein (EBNA1,

EBNA1ΔGAr, 235GAr-OVA or OVA) levels were normalized with respect to GAPDH (loading control) and the resulting values indicated below the gels.

On the basis of the compounds effect on the expression of EBNA1 and *in silico* evaluation of their drug-likeness, **PyDH2** and **PhenDH2** were selected for further biological studies that include antigen presentation assay and proximity ligation assay (PLA). For this purpose, we first evaluated the effect of various concentrations of both compounds on expression of ovalbumin (OVA) and 235GAr-OVA in H1299 cells using the same procedure as described above for EBNA1. The OVA/235GAr-OVA system allows to assess the ability of GAr to limit both protein expression and antigen presentation since 235GAr (a full-length, 235 amino-acid GAr domain), when fused to OVA, strongly limits both its expression and its antigen presentation by the MHC class I pathway. In this way, this model recapitulates the effect of GAr on EBNA1 expression and antigen presentation [18]. Similar to what has been observed with **PhenDC3** [22], compounds **PyDH2** and **PhenDH2** increased 235GAr-OVA level in a dose-dependent manner, whereas having no significant effect on OVA expression (Fig. 5b,c). Together with the data on the effect of compounds on EBNA1 expression, these results confirm the suggested mechanism of biological activity of both compounds, namely, relieving of the GAr-dependent inhibition of protein expression.

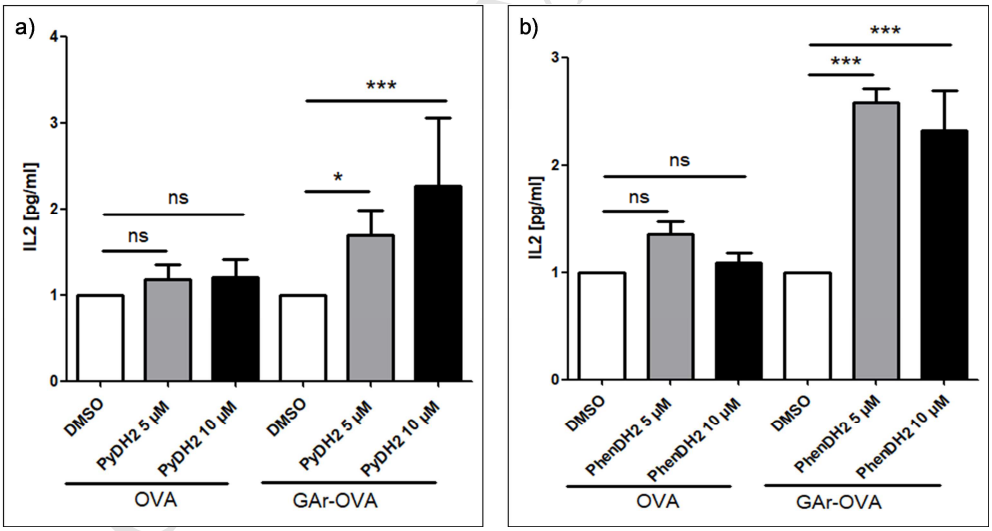

Fig. 6. IL2 concentration (pg mL^{-1}) determined following the treatment of H1299 cells expressing OVA (left) or GAr-OVA (right) with a) DMSO (control), 5 µM and 10 µM of **PyDH2**; b) DMSO (control), 5 µM and 10 µM of **PhenDH2**. *, $p < 0.05$; ***, $p < 0.001$; ns, not significant.

2.5.3. Cell viability

The toxicity of compounds **PyDH2** and **PhenDH2** for Mutu-1 (Epstein-Barr virus-related Burkitt lymphoma) cells in a concentration range of 0.5 to 100 µM was assessed using the classical MTT assay and compared to the result obtained with cells treated by DMSO (compound vehicle). Upon 24

h treatment, both compounds displayed a relatively low toxicity for Mutu-1 cells (**PyDH2**: GI_{50} > 100 µM, **PhenDH2**: 50 < GI_{50} < 100 µM, Fig. 7). Moreover, the toxicity of both compounds was only slightly higher upon 48 h treatment (**PyDH2**: GI_{50} ≥ 100 µM, **PhenDH2**: GI_{50} ≈ 20 µM, cf. Supporting Information, Fig. S3). Thus, both compounds are not significantly toxic when used at a concentration range in which they increase the expression of EBNA1 and the production of EBNA1-derived antigenic peptides (i.e., 5–10 µM), in contrast to the prototype drug **PhenDC3**, which induced significant toxicity when used at concentrations > 2.5 µM in identical conditions [22]. Thus, as compared to the prototype G4 ligand **PhenDC3**, these novel acylhydrazone ligands present the advantage of being significantly less toxic.

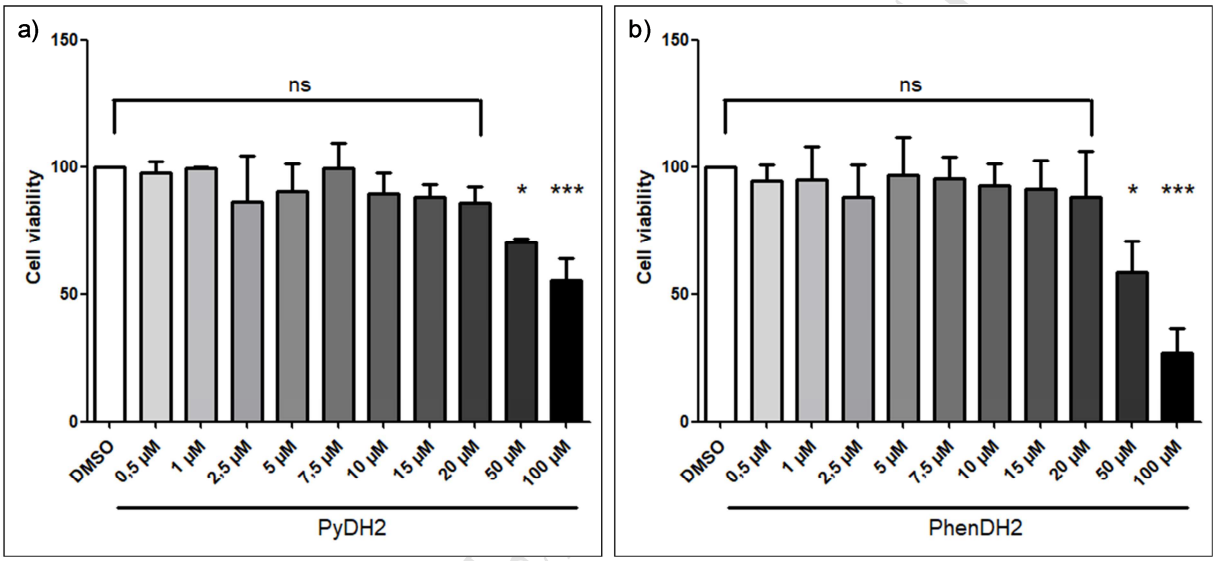

Fig. 7. Viability (%) of Mutu-1 cells assessed after a 24 h treatment with DMSO (control) or various concentrations of a) **PyDH2** or b) **PhenDH2**. *, $p < 0.05$; ***, $p < 0.001$; ns, not significant.

2.5.4. Inhibition of NCL binding to G4 in EBNA1 mRNA: proximity ligation assay (PLA) and RNA pull-down assay

We employed the proximity ligation assay (PLA) [40] to verify that compounds **PyDH2** and **PhenDH2** prevent nucleolin (NCL) to interact with the G4s of the GAr-encoding sequence of EBNA1 mRNA, the mechanism at the basis of the GAr-dependent limitation of EBNA1 expression and antigen presentation. Briefly, PLA is a technique originally developed to detect proteins in close proximity (theoretically, at a maximum distance of 40 nm) and which is based on the use of a pair of antibodies raised in two different species, each targeting one of the two protein of interest. By using labelled oligomers, PLA has been adapted to the study of protein–DNA [41] and protein–RNA interactions. In the latter case, mRNA of interest (i.e., EBNA1) is tagged through *in situ* hybridization with a digoxigenin-labelled DNA probe, followed by incubation with a mouse anti-digoxigenin, whereas NCL is tagged with rabbit anti-nucleolin. If both are located in a close proximity, the subsequent

incubation with DNA probe-conjugated anti-rabbit (*plus* probe) and anti-mouse (*minus* probe) antibodies and two connector oligonucleotide probes induces rolling circle amplification, as schematically shown on Fig. S4 (Supporting Information). The latter generates a concatemeric DNA product, which is finally detected thorough hybridization with a fluorescently labelled oligonucleotide probe as a distinct bright spot on a micrograph [42]. This way, we previously demonstrated that NCL interacts with G-quadruplexes formed in the GAr-encoding sequence of EBNA1 mRNA, and that **PhenDC3** inhibits this interaction in Mutu-1 cells as well as in H1299 cells transiently expressing EBNA1 [22,42]. Herein, we first exploited H1299 cells transiently expressing EBNA1 following transfection with EBNA1 plasmid. Cells treated with DMSO control demonstrated high level of PLA signals (1.83 ± 0.54 per cell) further confirming that the EBNA1 mRNA–NCL interaction takes place in, or at the close vicinity of the nucleus (Fig. 8a), whereas non-transfected cells did not display PLA signals (Supplementary Fig. S5). Treatment with compounds **PyDH2** or **PhenDH2** both at a concentration of 5 µM significantly reduced both the number (0.27 ± 0.11 and 0.40 ± 0.21 per cell, in cells treated with **PyDH2** and **PhenDH2**, respectively) and the intensity of PLA signals (Fig. 8b–d), hence confirming the ability of these new derivatives to disrupt the EBNA1 mRNA–NCL interaction, *in fine* leading to the GAr-dependent inhibition of EBNA1 expression and presentation of EBNA1-derived antigenic peptides. A similar effect was observed in Mutu-1 cells (EBV-infected Burkitt lymphoma B cells expressing endogenous EBNA1): treatment with 5 µM **PhenDH2** decreased the average number of PLA signals per cell from 1.68 ± 0.44 to 0.59 ± 0.20 (Fig. 9 and Supplementary Fig. S6).

Finally, to confirm that both hit compounds interfere with NCL binding to G4 structures in EBNA1 mRNA, we performed *in vitro* RNA pull-down assay using biotin-tagged RNA oligonucleotide g4-EBNA1 and recombinant NCL. Experiments performed in the presence of **PyDH2** or **PhenDH2** (10 µM) demonstrated that both compounds reduced the amount of RNA-bound NCL almost 10-fold with respect to DMSO control (Fig. 10a); in identical conditions, **PhenDC3** employed at the same concentration reduced the amount of bound NCL only two-fold [22]. Of note, negligible binding of NCL was detected with a non-G4-forming RNA oligonucleotide GM (obtained from g4-EBNA1 by replacement of guanines critical for G4 formation with A or U residues), demonstrating that RNA binding of NCL is G4-specific (Fig. 10b). Collectively, these results strongly suggest that **PyDH2** and **PhenDH2**, similarly but more efficiently than **PhenDC3**, act by preventing NCL to interact with G4s that form in the GAr-encoding sequence of EBNA1 mRNA.

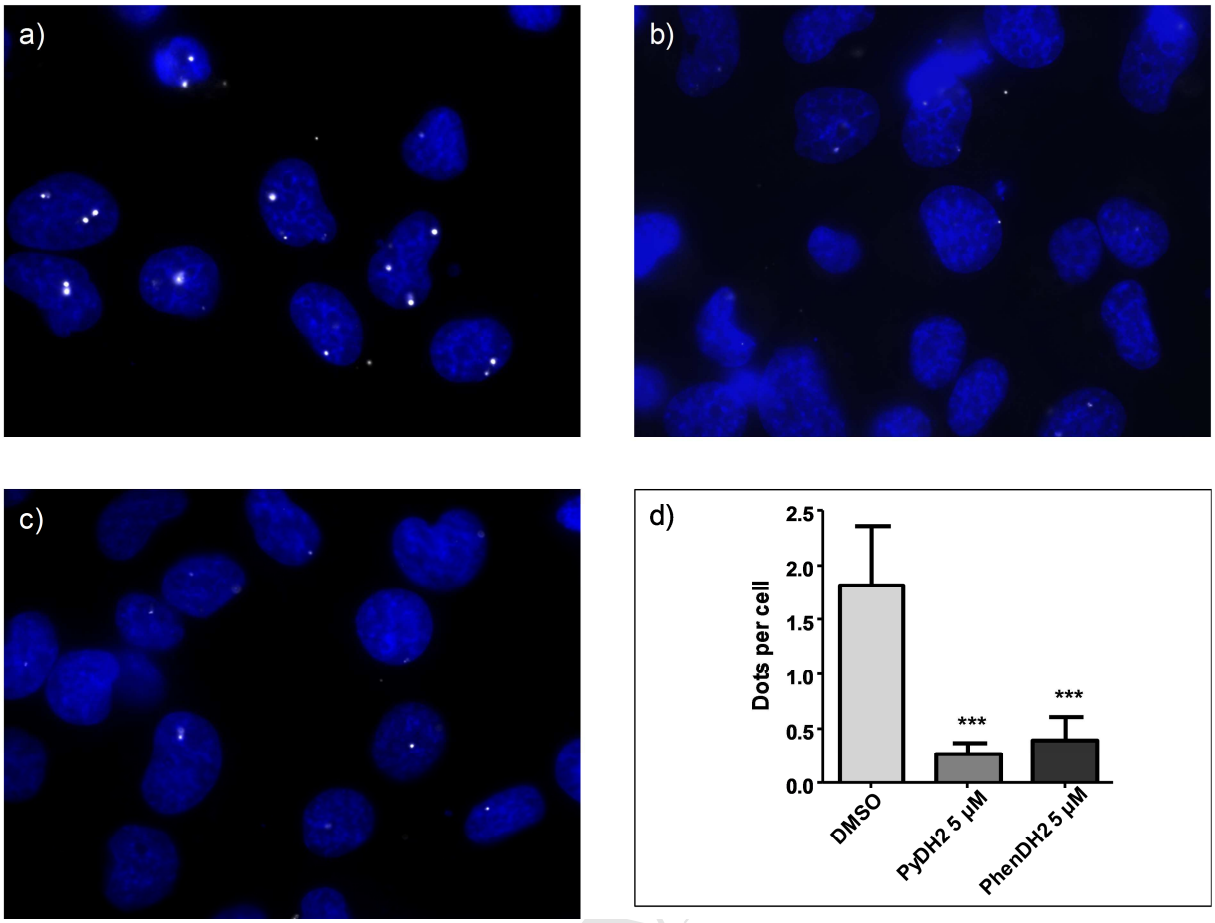

Fig. 8. Proximity ligation assay (PLA) performed in H1299 cells transiently expressing EBNA1. a–c) Microscopy images of cells treated with a) DMSO (compound vehicle, negative control), b) **PyDH2** (5 µM), and c) **PhenDH2** (5 µM). Nuclei were revealed by DAPI staining and appear in blue; white dots (PLA signals) indicate interaction between NCL and G4 of EBNA1 mRNA. As previously observed, this interaction mostly takes place in, or at the close vicinity of the nucleus [22,42]. d) Number of nuclear PLA signals (dots) per cell in H1299 cells expressing EBNA1 and treated with DMSO (control), **PyDH2** (5 µM) or with **PhenDH2** (5 µM). Data from two biological replicates, 100 cells per sample were analyzed. ***, $p < 0.001$.

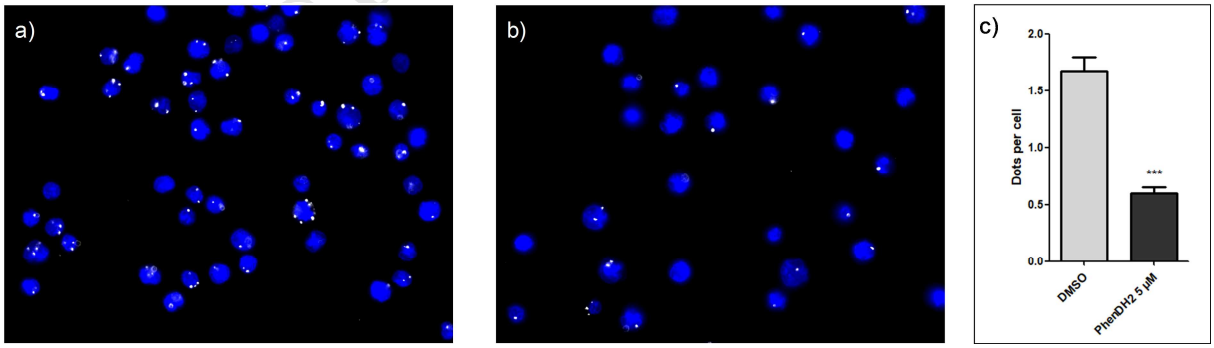

Fig. 9. Proximity ligation assay (PLA) performed in Mutu-1 cells natively expressing EBNA1. a–b) Microscopy images of cells treated with a) DMSO (compound vehicle, negative control) and b) **PhenDH2** (5 µM). Nuclei were revealed by DAPI staining and appear in blue; white dots (PLA signals) indicate interaction between NCL and G4 of EBNA1 mRNA. c) Number of nuclear PLA signals (dots) per cell in Mutu-1 cells treated with DMSO

(control) or with **PhenDH2** (5 µM). Data from two biological replicates, ≥ 200 cells per sample were analyzed. ***, $p < 0.001$.

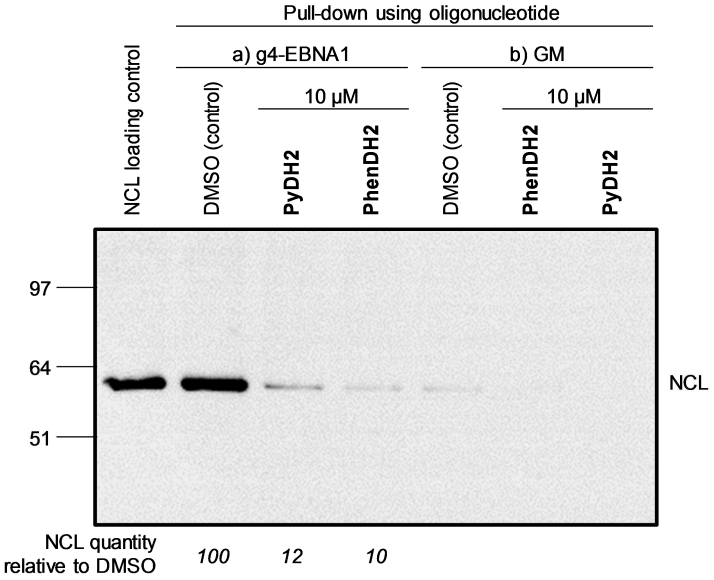

Fig. 10. RNA pulldown assay to identify the capacity of ligands to prevent NCL binding to G4-RNA. Recombinant NCL was applied to streptavidin-coupled agarose beads and biotin-tagged RNA oligonucleotides: a) g4-EBNA1; b) GM (non-G4-forming 18-mer sequence) in the presence of **PyDH2** or **PhenDH2** (at a concentration of 10 µM) or DMSO (vehicle) as indicated. The NCL protein still bound to the beads after washing with 800 mM KCl was eluted (SDS buffer) and analyzed by SDS-PAGE and western blot.

3. DISCUSSION

3.1. *In vitro* binding to g4-EBNA1: structure–properties relationships

A systematic comparison of 20 derivatives belonging to the same bis(acylhydrazone) family allowed us to reveal several interesting relationships between the structure of ligands and their affinity to g4-EBNA1. Firstly, the core heterocycle (Ar^1) proved to play a crucial role, as all PymDH derivatives exhibited poor ability to bind and stabilize g4-EBNA1, as demonstrated by the results of both biophysical techniques (FID assay and fluorescence melting). As evidenced by X-ray structural analysis (Fig. 2), this is due to the extended linear shape of PymDH derivatives, which ostensibly hampers their efficient stacking with G-quartets. Considering the whole set of ligands, the following trend can be deduced with respect to the impact of Ar^1 on G4-binding properties: PhenDH > NaphDH ≈ PyDH >> PymDH. A similar trend, albeit not comprising pyrimidine derivatives, was also observed in other series of related cationic dicarboxamide derivatives [43,44]. Secondly, within each sub-family of ligands, derivatives with lateral pyridinium residues (i.e., **PyDH1**, **PymDH1**, **NaphDH1**, and **PhenDH1**) systematically demonstrated less efficient binding to G4 structures, in contrast to the derivatives bearing lateral quinolinium heterocycles. Consistently with literature data on related

derivatives [43], this fact can be attributed to the limited π-stacking surface of pyridinium derivatives. With respect to the substitution pattern of lateral quinolinium rings, 4-substituted derivatives (**PyDH3** etc.) appeared more efficient g4-EBNA1 binders than analogous, 6-substituted derivatives (**PyDH5** etc.) according to the FID assay, but this trend was not supported by the results of the fluorescence-melting assay. Finally, side-chain substituents (R) seem to have little influence on G4-binding properties, even though their impact could not be comprehensively evaluated due to the limited size of our combinatorial matrix. On the other hand, the nature of these substituents plays a crucial role for bioavailability of bis(acylhydrazones), with benzyl substituents are detrimental to drug-like properties due to imparted high molecular weight and insaturation. Of note, the same structure–properties relationships were observed with respect to ligand-induced stabilization of two G4-DNA substrates, myc22 (parallel G4-DNA) and 25TAG (hybrid G4-DNA), demonstrating the polyvalence of G4-binding properties of the novel ligands. Thus, the *N*-acylhydrazone group appears to be essentially as efficient as the carboxamide group in the design of cationic poly-heteroaromatic G4 ligands, as can be evidenced from comparison of the results obtained with **PhenDC3** and its acylhydrazone analogue **PhenDH2** (the former appears as a slightly more efficient binder in fluorescence melting assay, but not in the FID assay). Taken together, these data demonstrate that cationic bis(acylhydrazones) represent a promising scaffold for G4-DNA and G4-RNA binders, providing wide possibilities for further functionalization and modulation of physico-chemical properties.

3.2. Effect of compounds on the GAr-dependent synthesis of EBNA1 and immune evasion of EBV

Among the 20 tested bis(acylhydrazones, **PyDH2** and **PhenDH2** were found to increase EBNA1 expression in a GAr-dependent manner in H1299 cells (Table 2). Remarkably, both compounds demonstrated high affinity to g4-EBNA1 according to two biophysical methods (fluorescence melting and FID assay, Fig. 4). These results speak in favor of the expected mechanism for their biological activity, namely, interference with the NCL-based inhibition of mRNA translation by preventing the interaction between NCL and G4 structures in EBNA1 mRNA, as further confirmed by PLA and RNA pull-down assays. Considering the absence of selective targeting of G4-RNA with respect to G4-DNA *in vitro*, the cellular activity of the two compounds can be attributed to the fact that GAr repeat of EBNA1 mRNA contains a cluster of multiple (≈13) G4-forming sequences, which may be particularly susceptible to ligand-induced effects such as NCL displacement. Moreover, G4-DNA structures form only transiently during DNA transactions such as replication, transcription and recombination, and are otherwise disfavored in the double-stranded DNA context; this is not the case with RNA whose single-stranded nature favors the formation of long-lived secondary motifs such as G4. PLA experiments provided further support this mechanism, demonstrating the ability of compounds to

disrupt the interaction between NCL and the GAr-encoding sequence of EBNA1 mRNA in cells. Consistently, both compounds were found to increase expression of 235GAr-OVA and the level of antigen presentation in the GAr-OVA model, while having no effect on cells expressing OVA. Considering their low intrinsic toxicity with respect to Mutu-1 cells (**PyDH2**: GI_{50} > 100 µM, **PhenDH2**: 50 > GI_{50} > 100 µM), both compounds may be employed in order to overcome the immune evasion of EBV through reversion of NCL and GAr-based repression of EBNA1 expression.

Interestingly, four naphthyridine derivatives (**NaphDH2–5**) demonstrated significant stabilization of g4-EBNA1, according to fluorescence melting experiments (Fig. 4a), but had not influence on EBNA1 expression (Table 2). This behavior is not without precedent, as it was also observed with pyridostatin (PDS), another well-studied G4 binder [22], and indicates that ligand-induced stabilization of a G4 structure is not a prerequisite to prevent its interaction with NCL by a competitive mechanism. In fact, one can imagine that stabilization of G4 structure could even favor their interaction with NCL (cf. Fig. S3, Supporting Information). Hence, G4 stabilization and ability to interfere with NCL–G4 interaction may be two independent events. In line, all NaphDH derivatives were significantly less active in displacing the fluorescence probe TO from g4-EBNA1 (DC_{50} > 0.5 µM), in contrast to the two biologically active derivatives, **PyDH2** and **PhenDH2** (Fig. 4b). This also indicates that FID assay is potentially better suited for identification of G4-targeting drugs acting through interference with protein binding to G4 structures. Therefore, the different compounds described here, in addition to constitute promising scaffolds for drugs able to unveil EBV-related tumors to the immune system and more generally to interfere with G4-RNA binders, may also represent useful tools to decipher the mode of interaction between cellular factors and G4.

The final aspect of his works is related to the potential applications of G4 ligands in the context of EBV-related cancers. Indeed, since most of EBV-infected individuals does not develop EBV-linked cancers, it is important to consider the putative effect of drugs on the virus latency, irrespectively of the obvious application for treating cancers associated to EBV infection. However, in healthy individuals, the latent infection by EBV is primarily restricted to a specific small pool of memory B cells. Hence, overcoming the GAr-based inhibition of EBNA1 translation, in addition to unveil EBV-carrying tumor cells to cytotoxic T cells, should also unveil just a few non-tumoral cells, therefore having no effect on the vast majority of healthy host cells. The second point is that, because our compounds should unveil all EBV-infected cells to the immune system (given that EBNA1 is expressed in all EBV-infected cells as it is essential for viral genome replication and maintenance), they would most certainly have applications as anti-viral agents, thereby probably presenting interesting medical application in fields other than EBV-related cancers. For example, they may find applications in grafted patients that all receive immunosuppressive treatments after the graft, which may lead to

reactivation of EBV thereby leading to lympho-proliferation. In these patients, elimination of EBV-infected cells prior to the graft may thus present a clear therapeutic interest.

4. CONCLUSION

In this work, we designed and synthesized a novel series of cationic derivatives representing bis(acylhydrazone) analogues of the well-studied G-quadruplex ligands PDC (360A) and **PhenDC3**. We demonstrated that harnessing the bis(acylhydrazone) motif allows facile generation of series of derivatives differing in terms of their physico-chemical properties, drug-like character, G4-binding properties, and biological activity. Specifically, our results demonstrate that the acylhydrazone group does not significantly impart the G4-binding properties of compounds, as compared with carboxamide analogues: instead, the binding to G4 structures seems mostly governed by the nature of central and lateral heterocyclic residues, revealing interesting SARs that can be interpreted in terms of molecular structure and preorganization of ligands. Even though the modifications of the scaffold explored in this work were not sufficient to achieve preferential targeting of viral G4-RNA with respect to G4-DNA *in vitro*, the results of biological assays demonstrate that two compounds, namely **PyDH2** and **PhenDH2**, displayed promising biological activity in EBV-related cellular models, being able to interfere with the GAr-dependent limitation of protein expression and antigen presentation. Moreover, both compounds were significantly less toxic than the prototype drug **PhenDC3** when used at concentrations required for boosting the production of EBNA1-derived antigenic peptides (i.e., 5–10 µM). Therefore, these compounds represent promising drug candidates for interfering with the immune evasion of EBV. Last but not least, the modular bis(acylhydrazone) scaffold presented here represents a promising platform for the development of novel ligands targeting other therapeutically important G4-RNA and/or G4-DNA structures.

5. EXPERIMENTAL SECTION

5.1. Chemistry

Synthesis and characterization: All commercially available chemicals were reagent grade and used without further purification. NMR spectra were measured with a Bruker Avance 300 spectrometer (^{1}H: 300 MHz, ^{13}C: 75 MHz) at 25 °C; chemical shifts are given in ppm (δ) values. Multiplicities of ^{13}C NMR signals were determined from DEPT-135 experiments. The melting points were determined in open-end capillaries with a digital melting point instrument (SMP30, Stuart). Elemental microanalysis of all novel compounds was performed by the *Service de Microanalyse*, CNRS–ICSN, Gif-sur-Yvette, France. The purity of final compounds was assessed by LC/MS analysis (Waters Alliance 2695 equipped with a Waters XBridge C_{18}-3.5 µm column and a photodiode array detector; eluent A: water with 0.05% TFA, eluent B: MeCN with 0.05% TFA, gradient elution with 2 to 100% of eluent B). Mass

spectra (MS, ESI in the positive-ion mode) were recorded with a Waters ZQ instrument (cone voltage: 30 V). In the assignment of MS of salts, *M* always refers to the organic dication.

General procedure for the synthesis of bis(acylhydrazides) (1–4): A solution of the corresponding dimethyl ester (1.95 g, 10 mmol) and hydrazine hydrate (10.9 mL, 11.2 g, 220 mmol) in ethanol (150 mL) was heated under reflux for 18 h and then cooled to room temperature. The precipitate was filtered, washed twice with ethanol, once with ether, and dried, to give the bis(acylhydrazide) which was sufficiently pure and employed without further purification.

*Pyridine-2,6-dicarbohydrazide (**1**)* [45]: Yield 1.73 g (89%). White solid, m.p. 285–286 °C (lit. 285 °C); ^{1}H NMR (300 MHz, DMSO-d_6): δ 10.63 (s, 2H), 8.13 (s, 3H), 4.63 (br s, 4H); ^{13}C NMR (75 MHz, DMSO-d_6): δ 161.9 (C_q), 148.4 (C_q), 139.3 (CH), 123.7 (CH); MS (ESI$^+$): m/z = 196.2 $[M + H]^+$.

*Pyrimidine-4,6-dicarbohydrazide (**2**):* Yield 1.81 g (92%). Pale-yellow solid, m.p. (decomp.) 280 °C; ^{1}H NMR (300 MHz, DMSO-d_6): δ 10.41 (s, 2H), 9.35 (d, J = 1.1 Hz, 1H), 8.35 (d, J = 1.1 Hz, 1H), 4.77 (br s, 4H); ^{13}C NMR (75 MHz, DMSO-d_6): δ 160.1 (C_q), 158.4 (C_q), 157.2 (CH), 114.7 (CH); MS (ESI$^+$): m/z = 197.1 $[M + H]^+$.

*1,8-Naphthyridine-2,7-dicarbohydrazide (**3**):* Yield 2.45 g (97%). Pale-yellow solid, m.p. > 290 °C; ^{1}H NMR (300 MHz, DMSO-d_6): δ 10.00 (s, 2H), 8.74 (d, J = 8.4 Hz, 2H), 8.25 (d, J = 8.4 Hz, 2H), 4.74 (br s, 4H); ^{13}C NMR (75 MHz, CD_3CO_2D): δ 164.7 (C_q), 153.1 (C_q), 141.1 (CH), 126.7 (C_q), 122.0 (CH); MS (ESI$^+$): m/z = 247.1 $[M + H]^+$.

*1,10-Phenanthroline-2,9-dicarbohydrazide (**4**)* [46]: Yield 2.38 g (80%). Pale yellow solid, m.p. > 290 °C (lit. 318–325 °C); ^{1}H NMR (300 MHz, DMSO-d_6): δ 10.77 (s, 2H), 8.69 (d, J = 8.3 Hz, 2H), 8.40 (d, J = 8.3 Hz, 2H), 8.14 (s, 2H), 4.78 (br s, 4H); ^{13}C NMR (75 MHz, DMSO-d_6): δ 162.9 (C_q), 149.5 (C_q), 144.0 (C_q), 137.9 (CH), 130.1 (C_q), 127.8 (CH), 121.0 (CH); MS (ESI$^+$): m/z = 297.2 $[M + H]^+$.

Typical procedure for the synthesis of bis(acylhydrazone) precursors (6a–c, 7a–c, 8a–c, and 9a–c): A solution of a bis(acylhydrazide) (**1–4**, 2.0 mmol) and a heteroaromatic aldehyde (**5a–5c**, 4.4 mmol) in ethanol (10 mL) was heated under reflux for 18 h. After cooling, the precipitate was collected by filtration, thoroughly washed with ethanol, and dried, to give the corresponding bis(acylhydrazone) which was sufficiently pure and employed without further purification.

*N'^2,N'^6-Bis(pyridin-4-ylmethylene)pyridine-2,6-dicarbohydrazide (**6a**):* Yield 90%; white powder, m.p. > 290 °C; ^{1}H NMR (300 MHz, DMSO-d_6): δ 12.54 (s, 2H), 8.79 (s, 2H), 8.72 (d, J = 5.9 Hz, 4H), 8.44–8.25

(m, 3H), 7.77 (d, J = 6.0 Hz, 4H); ^{13}C NMR (75 MHz, DMSO-d_6): δ 159.8 (C_q), 150.4 (CH), 148.0 (C_q), 147.6 (CH), 141.3 (C_q), 140.2 (CH), 125.9 (CH), 121.1 (CH); MS (ESI$^+$): m/z = 374.2 [M + H]$^+$, 187.7 [M + 2H]$^{2+}$.

*N'²,N'⁶-Bis(quinolin-4-ylmethylene)pyridine-2,6-dicarbohydrazide (**6b**):* Yield 93%; pale-yellow solid, m.p. > 290 °C; ^{1}H NMR (300 MHz, DMSO-d_6): δ 12.65 (s, 2H), 9.48 (s, 2H), 9.07 (d, J = 4.5 Hz, 2H), 8.91 (dd, J = 8.4, 0.7 Hz, 2H), 8.53–8.33 (m, 3H), 8.16 (dd, J = 8.3, 0.7 Hz, 2H), 7.99 (d, J = 4.5 Hz, 2H), 7.92–7.79 (m, 4H); ^{13}C NMR (75 MHz, DMSO-d_6): δ 159.7 (C_q), 150.5 (CH), 148.5 (C_q), 148.0 (C_q), 147.3 (CH), 140.3 (CH), 137.1 (C_q), 129.9 (CH), 129.8 (CH), 127.7 (CH), 125.9 (CH), 124.8 (C_q), 124.4 (CH), 120.0 (CH); MS (ESI$^+$): m/z = 474.3 [M + H]$^+$.

*N'²,N'⁶-Bis(quinolin-6-ylmethylene)pyridine-2,6-dicarbohydrazide (**6c**):* Yield 80%; pale-yellow solid, m.p. > 290 °C; ^{1}H NMR (300 MHz, DMSO-d_6): δ 12.50 (s, 2H), 9.01–8.94 (m, 4H), 8.52 (d, J = 7.8 Hz, 2H), 8.46–8.39 (m, 2H), 8.39–8.28 (m, 5H), 8.13 (d, J = 8.8 Hz, 2H), 7.63 (dd, J = 8.3, 4.3 Hz, 2H); ^{13}C NMR (75 MHz, DMSO-d_6): δ 159.6 (C_q), 151.5 (CH), 149.2 (CH), 148.6 (C_q), 148.2 (C_q), 140.1 (CH), 136.5 (CH), 132.3 (C_q), 129.8 (CH), 129.0 (CH), 128.0 (C_q), 126.4 (CH), 125.6 (CH), 122.2 (CH); MS (ESI$^+$): m/z = 474.3 [M + H]$^+$, 237.7 [M + 2H]$^{2+}$.

*N'⁴,N'⁶-Bis(pyridin-4-ylmethylene)pyrimidine-4,6-dicarbohydrazide (**7a**):* Yield 99%; white solid, m.p. > 290 °C; ^{1}H NMR (300 MHz, DMF-d_7): δ 12.77 (s, 2H), 9.60 (s, 1H), 8.89 (s, 2H), 8.80–8.70 (m, 5H), 7.79 (d, J = 6.0 Hz, 4H); ^{13}C NMR (75 MHz, DMF-d_7): δ 159.7 (C_q), 159.1 (C_q), 158.0 (CH), 150.9 (CH), 148.8 (CH), 141.9 (C_q), 121.6 (CH), 116.8 (CH); MS (ESI$^+$): m/z = 375.2 [M + H]$^+$, 188.1 [M + 2H]$^{2+}$.

*N'⁴,N'⁶-Bis(quinolin-4-ylmethylene)pyrimidine-4,6-dicarbohydrazide (**7b**):* Yield 99%; pale-yellow solid, m.p. (decomp.) 282 °C; ^{1}H NMR (300 MHz, DMF-d_7): δ 12.89 (s, 2H), 9.68 (d, J = 10.9 Hz, 3H), 9.10 (d, J = 4.4 Hz, 2H), 8.93–8.79 (m, 3H), 8.18 (d, J = 8.2 Hz, 2H), 8.02 (s, 2H), 7.96–7.86 (m, 2H), 7.86–7.76 (m, 2H); ^{13}C NMR (75 MHz, DMF-d_7): δ 160.0 (C_q), 157.7 (CH), 150.4 (CH), 149.5 (C_q), 148.4 (CH), 137.9 (C_q), 130.3 (CH), 129.5 (CH), 127.6 (CH), 125.6 (C_q), 124.6 (CH), 123.4 (C_q) 120.3 (CH), 116.8 (CH); MS (ESI$^+$): m/z = 475.3 [M + H]$^+$, 238.2 [M + 2H]$^{2+}$.

*N'⁴,N'⁶-Bis(quinolin-6-ylmethylene)pyrimidine-4,6-dicarbohydrazide (**7c**):* Yield 99%; pale-yellow solid, m.p. > 290 °C; ^{1}H NMR (300 MHz, DMSO-d_6): δ 12.68 (s, 2H), 9.60 (s, 1H), 9.03–8.87 (m, 4H), 8.65 (s, 1H), 8.51 (d, J = 8.0 Hz, 2H), 8.32–8.20 (m, 4H), 8.10 (d, J = 8.4 Hz, 2H), 7.66–7.55 (m, 2H).; ^{13}C NMR (75 MHz, CD_3CO_2D): δ 160.2 (C_q), 158.6 (C_q), 158.0 (CH), 150.5 (CH), 147.1 (CH), 145.2 (CH), 141.5 (C_q), 134.7 (C_q), 131.0 (CH), 130.6 (CH), 129.0 (C_q), 123.7 (CH), 123.0 (CH), 116.9 (CH); MS (ESI$^+$): m/z = 475.3 [M + H]$^+$, 238.2 [M + 2H]$^{2+}$.

*N'²,N'⁷-Bis(pyridin-4-ylmethylene)-1,8-naphthyridine-2,7-dicarbohydrazide (**8a**):* Yield 78%; white solid, m.p. > 290 °C; ^{1}H NMR (300 MHz, DMSO-d_6): δ 12.63 (s, 2H), 8.89 (d, *J* = 8.3 Hz, 2H), 8.81–8.58 (m, 6H), 8.42 (d, *J* = 8.3 Hz, 2H), 7.71 (d, *J* = 4.6 Hz, 4H); ^{13}C NMR (75 MHz, CD_3CO_2D): *δ* 162.7 (C_q), 153.5 (C_q), 149.3 (C_q), 147.1 (CH), 145.3 (CH), 141.5 (CH), 127.7 (C_q), 124.8 (CH), 123.1 (CH); MS (ESI$^+$): *m*/*z* = 425.3 [*M* + H]$^+$.

*N'²,N'⁷-Bis(quinolin-4-ylmethylene)-1,8-naphthyridine-2,7-dicarbohydrazide (**8b**):* Yield 80%; white solid, m.p. > 290 °C; ^{1}H NMR (300 MHz, DMSO-d_6): *δ* 12.72 (s, 2H), 9.51 (s, 2H), 9.05 (d, *J* = 4.5 Hz, 2H), 8.93 (d, *J* = 8.3 Hz, 2H), 8.78 (d, *J* = 8.3 Hz, 2H), 8.48 (d, *J* = 8.3 Hz, 2H), 8.14 (d, *J* = 8.2 Hz, 2H), 7.95 (d, *J* = 4.4 Hz, 2H), 7.91–7.84 (m, 2H), 7.84–7.77 (m, 2H); ^{1}H NMR (300 MHz, CD_3CO_2D/D_2O 1:1 v/v): *δ* 9.36 (s, 2H), 9.02 (d, *J* = 5.5 Hz, 2H), 8.67–8.55 (m, 4H), 8.36 (dd, *J* = 13.8, 7.0 Hz, 4H), 8.11 (d, *J* = 8.4 Hz, 2H), 7.99–7.90 (m, 2H), 7.90–7.80 (m, 2H); ^{13}C NMR (75 MHz, CD_3CO_2D/D_2O 1:1 v/v): *δ* 162.0 (C_q), 152.7 (C_q), 145.6 (CH), 144.5 (CH), 141.2 (CH), 141.0 (C_q), 134.5 (CH), 130.8 (CH), 127.1 (C_q), 126.4 (C_q), 124.9 (CH), 123.6 (CH), 122.6 (CH), 119.7 (CH); MS (ESI$^+$): *m*/*z* = 525.2 [*M* + H]$^+$, 263.2 [*M* + 2H]$^{2+}$.

*N'²,N'⁷-Bis(quinolin-6-ylmethylene)-1,8-naphthyridine-2,7-dicarbohydrazide (**8c**):* Yield 80%; white solid, m.p. > 290 °C; ^{1}H NMR (300 MHz, DMSO-d_6): *δ* 12.56 (s, 2H), 9.07–8.74 (m, 6H), 8.52 (d, *J* = 8.3 Hz, 2H), 8.44 (d, *J* = 8.2 Hz, 2H), 8.33–8.25 (m, 4H), 8.12 (d, *J* = 8.9 Hz, 2H), 7.62 (dd, *J* = 7.6, 4.0 Hz, 2H); ^{13}C NMR spectrum could not be obtained due to insufficient solubility; MS (ESI$^+$): *m*/*z* = 263.1 [*M* + 2H]$^{2+}$.

*N'²,N'⁹-Bis(pyridin-4-ylmethylene)-1,10-phenanthroline-2,9-dicarbohydrazide (**9a**):* Yield 77%; pale yellow solid, m.p. > 290 °C; ^{1}H NMR (300 MHz, DMF-d_7): *δ* 12.87 (s, 2H), 9.11 (s, 2H), 8.92 (d, *J* = 8.3 Hz, 2H), 8.81 (d, *J* = 5.8 Hz, 4H), 8.67 (d, *J* = 8.3 Hz, 2H), 8.34 (s, 2H), 7.85 (d, *J* = 5.8 Hz, 4H); NMR (75 MHz, DMF-d_7): *δ* 161.1 (C_q), 150.9 (CH), 149.8 (C_q), 147.9 (CH), 144.6 (C_q), 142.4 (C_q), 139.0 (CH), 131.5 (C_q), 128.8 (CH), 122.1 (CH), 121.6 (CH); MS (ESI$^+$): *m*/*z* = 475.3 [*M* + H]$^+$.

*N'²,N'⁹-Bis(quinolin-4-ylmethylene)-1,10-phenanthroline-2,9-dicarbohydrazide (**9b**):* Yield 55%; pale yellow solid, m.p. > 290 °C; ^{1}H NMR (300 MHz, DMSO-d_6): *δ* 12.97 (s, 2H), 9.62 (s, 2H), 8.86–8.83 (m, 4H), 8.65 (d, *J* = 8.3 Hz, 2H), 8.61 (d, *J* = 8.2 Hz, 2H), 8.26 (s, 2H), 7.99 (d, *J* = 8.3 Hz, 2H), 7.81 (d, *J* = 4.5 Hz, 2H), 7.61–7.53 (m, 2H), 7.10–7.02 (m, 2H); ^{13}C NMR (75 MHz, DMSO-d_6): *δ* 160.4 (C_q), 150.1 (CH), 149.0 (C_q), 148.1 (C_q), 147.3 (CH), 138.8 (CH), 138.1 (CH), 137.8 (C_q), 130.9 (C_q), 129.4 (CH), 129.4 (CH), 128.6 (CH), 126.9 (CH), 124.9 (CH), 124.2 (C_q), 122.0 (CH), 119.6 (CH); MS (ESI$^+$): *m*/*z* = 575.3 [*M* + H]$^+$, 288.2 [*M* + 2H]$^{2+}$.

*N'²,N'⁹-Bis(quinolin-6-ylmethylene)-1,10-phenanthroline-2,9-dicarbohydrazide (**9c**):* Yield 59%; pale yellow solid, m.p. > 290 °C; ^{1}H NMR (300 MHz, DMF-d_7): *δ* 12.88 (s, 2H), 9.37 (s, 2H), 9.01 (dd, *J* = 4.2,

1.5 Hz, 2H), 8.93 (d, *J* = 8.3 Hz, 2H), 8.69 (d, *J* = 8.3 Hz, 2H), 8.48 (dd, *J* = 8.8, 1.6 Hz, 2H), 8.34 (d, *J* = 7.4 Hz, 4H), 8.19 (d, *J* = 8.8 Hz, 2H), 8.11 (d, *J* = 7.9 Hz, 2H), 7.53 (dd, *J* = 8.3, 4.2 Hz, 2H); ^{13}C NMR (75 MHz, DMF-d_7): δ 160.8 (C_q), 151.8 (CH), 150.0 (C_q), 149.5 (C_q), 149.5 (CH), 144.5 (C_q), 138.9 (CH), 136.6 (CH), 133.6 (C_q), 131.4 (C_q), 130.4 (CH), 129.3 (CH), 128.7 (CH), 128.6 (C_q), 127.0 (CH), 122.5 (CH), 122.0 (CH); MS (ESI$^+$): *m*/*z* = 575.3 $[M + H]^+$, 288.2 $[M + 2H]^{2+}$.

4-Formyl-1-methylpyridinium iodide (**10a**):[47] The mixture of pyridine-4-carboxaldehyde (5.4 mL, 6.10 g, 56.9 mmol) and methyl iodide (7.0 mL, 15.95 g, 112.4 mmol) in DCM (20 mL) was stirred for 72 h at room temperature under argon atmosphere. The precipitated solid was filtered and washed twice with DCM, to give **10a** (13.3 g, 94%) as an orange solid. ^{1}H NMR (300 MHz, D_2O): δ 8.80 (d, *J* = 6.5 Hz, 2H), 8.12 (d, *J* = 6.2 Hz, 2H), 6.21 (s, 1H), 4.39 (s, 3H); ^{13}C NMR (75 MHz, D_2O): δ 160.1 (C_q), 146.0 (CH), 125.7 (CH), 88.2 (CH), 48.5 (CH_3); MS (ESI$^+$): *m*/*z* (%) = 140.1 (100) $[M + H_2O]^+$.

General procedure for the synthesis of quaternized heterocyclic aldehydes (11a–b, 12a–b): The solution of aldehyde (10 mmol) and alkylating agent (100 mmol) in acetone (18 mL) was stirred at 60 °C for 18 h and then cooled to room temperature. The precipitated solid was filtered, washed twice with acetone, once with ether, and dried.

*4-Formyl-1-methylquinolinium iodide (**11a**):* Obtained from quinoline-4-aldehyde and methyl iodide in a 77% yield. Red solid, ^{1}H NMR (300 MHz, D_2O): δ 9.25 (d, *J* = 6.1 Hz, 1H), 8.63 (d, *J* = 8.4 Hz, 1H), 8.42 (d, *J* = 9.0 Hz, 1H), 8.24 (m, 2H), 8.04 (m, 1H), 6.87 (s, 1H), 4.66 (s, 3H); ^{13}C NMR (75 MHz, D_2O): δ 157.8 (C_q), 150.1 (CH), 139.5 (C_q), 135.9 (CH), 130.8 (CH), 127.4 (C_q), 127.1 (CH), 119.5 (CH), 118.5 (CH), 86.8 (CH), 46.3 (CH_3); MS (ESI$^+$): *m*/*z* (%) = 190.3 (100) $[M + H_2O]^+$, 172.1 (25) $[M]^+$.

*4-Formyl-1-benzylquinolinium bromide (**11b**):* Obtained from quinoline-4-aldehyde and benzyl bromide in an 81% yield. ^{1}H NMR (300 MHz, D_2O): δ 9.39 (d, *J* = 6.1 Hz, 1H), 8.63 (d, *J* = 7.9 Hz, 1H), 8.45–8.25 (m, 2H), 8.15–8.04 (m, 1H), 7.97 (m, 1H), 7.42 (s, 3H), 7.32 (s, 2H), 6.89 (s, 1H), 6.28 (s, 2H); ^{13}C NMR (75 MHz, D_2O): δ 158.7 (C_q), 149.9 (CH), 139.0 (C_q), 136.1 (CH), 133.4 (C_q), 130.8 (CH), 130.1 (CH), 129.9 (CH), 128.1 (C_q), 128.0 (CH), 127.4 (CH), 120.0 (CH), 118.7 (CH), 86.9 (CH), 61.8 (CH_2); MS (ESI$^+$): *m*/*z* (%) = 266.2 (100) $[M + H_2O]^+$, 248.2 (6) $[M]^+$.

*6-Formyl-1-ethylquinolinium iodide (**12a**):* Obtained from quinoline-6-aldehyde and ethyl iodide in a 73% yield. ^{1}H NMR (300 MHz, DMSO-d_6): δ 10.31 (s, 1H), 9.68 (d, *J* = 4.7 Hz, 1H), 9.48 (d, *J* = 8.3 Hz, 1H), 9.08 (d, *J* = 1.7 Hz, 1H), 8.79 (d, *J* = 9.2 Hz, 1H), 8.60 (dd, *J* = 9.2, 1.7 Hz, 1H), 8.31 (dd, *J* = 8.4, 5.8 Hz, 1H), 5.13 (q, *J* = 7.2 Hz, 2H), 1.62 (t, *J* = 7.2 Hz, 3H); ^{13}C NMR (75 MHz, DMSO-d_6): δ 191.9 (C_q),

151.5 (CH), 148.7 (CH), 139.7 (C_q), 135.6 (C_q), 134.4 (CH), 132.5 (CH), 129.6 (C_q), 123.5 (CH), 120.3 (CH), 53.5 (CH_2), 15.2 (CH_3); MS (ESI^+): *m*/*z* (%) = 204.2 (8) $[M + H_2O]^+$, 186.1 (100) $[M]^+$.

*6-Formyl-1-benzylquinolinium iodide (**12b**):* Obtained from quinoline-6-aldehyde and benzyl bromide in an 85% yield. ^{1}H NMR (300 MHz, DMSO-d_6): δ 10.26 (s, 1H), 9.85 (d, *J* = 5.8 Hz, 1H), 9.58 (d, *J* = 8.3 Hz, 1H), 9.10 (d, *J* = 1.5 Hz, 1H), 8.67 (d, *J* = 9.2 Hz, 1H), 8.54 (dd, *J* = 9.2, 1.7 Hz, 1H), 8.41 (dd, *J* = 8.4, 5.8 Hz, 1H), 7.40 (s, 5H), 6.42 (s, 2H); ^{13}C NMR (75 MHz, DMSO-d_6): δ 191.7 (C_q), 152.5 (CH), 149.6 (CH), 139.9 (C_q), 135.7 (C_q), 134.3 (CH), 133.6 (C_q), 132.8 (CH), 129.9 (CH), 129.1 (C_q), 128.8 (CH), 127.4 (CH), 123.7 (CH), 120.6 (C_q), 60.2 (CH_2); MS (ESI^+): *m*/*z* (%) = 266.3 (10) $[M + H_2O]^+$, 248.2 (100) $[M]^+$.

Synthesis of cationic bis(acylhydrazones) (PyDH1, PyDH2). Method A: A mixture of bis(acylhydrazone) precursor **6a** or **6b** (0.5 mmol), alkyl halogenide (75 mmol) and DMF (3 mL) was sealed in a tube and heated at 40 °C during 18 h. After cooling to room temperature, the precipitate was filtered and washed with DMF and diethyl ether, and dried in vacuum. The crude product was purified by recrystallization from boiling MeCN–H_2O. *Note: this method gave sufficiently pure products PyDH1 and PyDH2; however, in the case PymDH1, PymDH2, and NaphDH2, the mono-alkylated by-product could not be removed by recrystallization. Method B (below) was therefore preferred for the synthesis of all bis(acylhydrazones).*

*$N^{\prime 2}$,$N^{\prime 6}$-Bis[(1-methylpyridinium-4-yl)methylene]pyridine-2,6-dicarbohydrazide iodide (**PyDH1**):* Yield 279 mg (85%). Orange powder; ^{1}H NMR (300 MHz, DMSO-d_6): δ 12.93 (s, 2H), 9.03 (d, *J* = 5.9 Hz, 4H), 8.94 (s, 2H), 8.54–8.31 (m, 7H), 4.37 (s, 6H); ^{13}C NMR (75 MHz, DMSO-d_6): δ 160.3 (C_q), 148.8 (C_q), 147.6 (C_q), 146.1 (CH), 143.8 (CH), 140.6 (CH), 126.6 (CH), 124.3 (CH), 47.7 (CH_3); MS (ESI^+): *m*/*z* (%) = 402.3 (100) $[M - H]^+$, 201.7 (41) $[M]^{2+}$; purity (LC) 100%.

*$N^{\prime 2}$,$N^{\prime 6}$-Bis[(1-methylquinolinium-4-yl)methylene]pyridine-2,6-dicarbohydrazide iodide (**PyDH2**):* Yield 360 mg (95%). Orange powder; ^{1}H NMR (300 MHz, DMSO-d_6): δ 13.03 (s, 2H), 9.74 (s, 2H), 9.54 (d, *J* = 6.3 Hz, 2H), 9.07 (d, *J* = 8.5 Hz, 2H), 8.66–8.56 (m, 4H), 8.52 (d, *J* = 7.0 Hz, 2H), 8.48–8.43 (m, 1H), 8.42–8.33 (m, 2H), 8.27–8.18 (m, 2H), 4.68 (s, 6H); ^{13}C NMR (75 MHz, DMSO-d_6): δ 160.1 (C_q), 149.4 (CH), 147.6 (C_q), 147.0 (C_q), 143.4 (CH), 140.7 (CH), 139.1 (C_q), 135.3 (CH), 130.5 (CH), 126.7 (CH), 126.3 (C_q), 126.0 (CH), 120.0 (CH), 119.0 (CH), 45.7 (CH_3); MS (ESI^+): *m*/*z* (%) = 502.3 (100) $[M - H]^+$, 616.3 (9) $[M + CF_3COO]^+$; purity (LC) 90%.

Synthesis of cationic bis(acylhydrazones). Method B: The mixture of dicarbohydrazide **1–4** (0.5 mmol) and quaternized aldehyde **10a**, **11a–b**, or **12a–b** (1.1 mmol) in DMF (3 mL) was heated at 100 °C (80 °C for NaphDH5 and PhenDH5) for 2 h and then cooled to room temperature. The precipitate was collected by filtration, washed three times with MeCN, once with ether, dried and then additionally recrystallized from MeCN/H_2O. The yields are indicated for ^{1}H-NMR spectroscopically pure material prior to the final recrystallization step.

*$N^{\prime 2}$,$N^{\prime 6}$-Bis[(1-methylpyridinium-4-yl)methylene]pyridine-2,6-dicarbohydrazide iodide (**PyDH1**):* Yield 90%. The appearance and spectroscopic properties were identical with those described above; purity (LC): 100%; anal. calcd. for $C_{21}H_{21}I_2N_7O_2 \times 2\ H_2O$ (693.3): C 36.38, H 3.63, N 14.14; found: C 36.03, H 3.31, N 14.05.

*$N^{\prime 2}$,$N^{\prime 6}$-Bis[(1-methylquinolinium-4-yl)methylene]pyridine-2,6-dicarbohydrazide iodide (**PyDH2**):* Yield 76%. The appearance and spectroscopic properties were identical with those described above; purity (LC): 100%; anal. calcd. for $C_{29}H_{25}I_2N_7O_2 \times 3.5\ H_2O$ (820.4): C 42.46, H 3.93, N 11.95; found: C 42.46, H 3.59, N 11.60.

*$N^{\prime 2}$,$N^{\prime 6}$-Bis[(1-benzylquinolinium-4-yl)methylene]pyridine-2,6-dicarbohydrazide bromide (**PyDH3**):* Yield 93%. Yellow-orange powder; ^{1}H NMR (300 MHz, DMSO-d_6): δ 13.34 (s, 2H), 10.29 (s, 2H), 9.74 (d, J = 6.2 Hz, 2H), 9.06 (d, J = 8.5 Hz, 2H), 8.66 (d, J = 6.2 Hz, 2H), 8.62–8.50 (m, 4H), 8.49–8.38 (m, 1H), 8.31–8.23 (m, 2H), 8.19–8.11 (m, 2H), 7.41 (s, 10H), 6.42 (s, 4H); ^{13}C NMR (75 MHz, DMSO-d_6): δ 160.0 (C_q), 149.4 (CH), 148.3 (C_q), 147.8 (C_q), 143.1 (CH), 140.4 (CH), 138.2 (C_q), 135.5 (CH), 134.0 (C_q), 130.2 (C_q), 129.2 (CH), 128.9 (CH), 127.4 (CH), 127.2 (C_q), 127.0 (CH), 126.3 (CH), 120.0 (CH), 118.4 (CH), 59.9 (CH_2); MS (ESI$^+$): m/z (%) = 654.4 (34) $[M - H]^+$, 327.8 (100) $[M]^{2+}$; purity (LC): 100%; anal. calcd. for $C_{41}H_{33}Br_2N_8O_2 \times 1.5\ H_2O$ (842.6): C 58.44, H 4.31, N 11.64; found: C 58.28, H 4.28, N 11.62.

*$N^{\prime 2}$,$N^{\prime 6}$-Bis[(1-ethylquinolinium-6-yl)methylene]pyridine-2,6-dicarbohydrazide iodide (**PyDH4**):* Yield 92%. Pale brown solid; ^{1}H NMR (300 MHz, DMSO-d_6): δ 12.67 (s, 2H), 9.59 (d, J = 5.4 Hz, 2H), 9.38 (d, J = 8.3 Hz, 2H), 9.07 (s, 2H), 8.85 (s, 2H), 8.74 (q, J = 9.6 Hz, 4H), 8.45 (d, J = 7.1 Hz, 2H), 8.41–8.32 (m, 1H), 8.32–8.16 (m, 2H), 5.14 (q, J = 7.0 Hz, 4H), 1.66 (t, J = 7.0 Hz, 6H); ^{13}C NMR (75 MHz, DMSO-d_6): δ 160.0 (C_q), 149.7 (CH), 148.0 (C_q), 147.4 (CH), 147.1 (CH), 140.3 (CH), 138.1 (C_q), 135.2 (CH), 132.3 (CH), 130.1 (C_q), 129.9 (CH), 126.0 (CH), 123.2 (CH), 120.0 (CH), 53.3 (CH_2), 15.3 (CH_3); MS (ESI$^+$): m/z (%) = 644.3 (32) $[M + CF_3COO]^+$, 265.8 (100) $[M]^{2+}$; purity (LC): 100%; anal. calcd. for $C_{31}H_{29}I_2N_7O_2 \times 1.5\ H_2O$ (821.5): C 45.33, H 4.05, N 11.94; found: C 45.44, H 4.11, N 11.96.

*$N^{\prime 2}$,$N^{\prime 6}$-Bis[(1-benzylquinolinium-6-yl)methylene]pyridine-2,6-dicarbohydrazide bromide (**PyDH5**):* Yield 55%. Pale yellow solid; ^{1}H NMR (300 MHz, DMSO-d_6): δ 12.72 (s, 2H), 9.76 (d, J = 5.0 Hz, 2H), 9.48 (d, J = 8.3 Hz, 2H), 9.12 (s, 2H), 8.85 (s, 2H), 8.73–8.58 (m, 4H), 8.46–8.30 (m, 5H), 7.49–7.34 (m,

10H), 6.41 (s, 4H); ^{13}C NMR (75 MHz, DMSO-d_6): δ 159.9 (C_q), 150.6 (CH), 148.3 (CH), 148.1 (C_q), 146.9 (CH), 140.2 (CH), 138.3 (C_q), 135.4 (C_q), 133.8 (C_q), 132.6 (CH), 130.4 (C_q), 129.7 (CH), 129.1 (CH), 128.9 (CH), 127.5 (CH), 126.1 (CH), 123.3 (CH), 120.3 (CH), 60.0 (CH_2); MS (ESI$^+$): *m/z* (%) = 768.3 (59) [*M* + CF_3COO]$^+$, 327.8 (100) [*M*]$^{2+}$; purity (LC): 99%; anal. calcd. for $C_{41}H_{33}Br_2N_7O_2 \times 1.5\ H_2O$ (842.6): C 58.44, H 4.31, N 11.64; found: C 58.74, H 4.42, N 11.56.

N^{4},*N*^{6}*-Bis[(1-methylpyridinium-4-yl)methylene]pyrimidine-4,6-dicarbohydrazide iodide (**PymDH1**):* Yield 97%. Yellow-orange solid; ^{1}H NMR (300 MHz, DMSO-d_6): δ 13.31 (s, 2H), 9.67 (s, 1H), 9.01 (d, *J* = 6.5 Hz, 4H), 8.86 (s, 2H), 8.64 (s, 1H), 8.38 (d, *J* = 6.4 Hz, 4H), 4.35 (s, 6H); ^{13}C NMR (75 MHz, DMSO-d_6): δ 159.9 (C_q), 158.2 (C_q), 157.7 (CH), 148.6 (C_q), 146.0 (CH), 144.9 (CH), 124.5 (CH), 119.3 (CH), 47.7 (CH_3); MS (ESI$^+$): *m/z* (%) = 403.3 (35) [*M* – H]$^+$, 202.2 (100) [*M*]$^{2+}$; purity (LC): 100%; anal. calcd. for $C_{20}H_{20}I_2N_8O_2 \times H_2O$ (676.3): C 35.52, H 3.28, N 16.57; found: C 35.13, H 3.33, N 16.29.

N^{4},*N*^{6}*-Bis[(1-methylquinolinium-4-yl)methylene]pyrimidine-4,6-dicarbohydrazide iodide (**PymDH2**):* Yield 92%. Orange solid; ^{1}H NMR (300 MHz, DMSO-d_6): δ 13.28 (s, 2H), 9.75 (s, 1H), 9.70 (s, 2H), 9.51 (d, *J* = 6.2 Hz, 2H), 8.86 (d, *J* = 8.4 Hz, 2H), 8.73 (s, 1H), 8.60 (d, *J* = 8.7 Hz, 2H), 8.52 (d, *J* = 6.1 Hz, 2H), 8.40–8.32 (m, 2H), 8.25–8.16 (m, 2H), 4.67 (s, 6H); ^{13}C NMR (75 MHz, DMSO-d_6): δ 159.6 (C_q), 158.0 (C_q), 157.8 (CH), 149.4 (CH), 146.7 (C_q), 144.3 (CH), 139.0 (C_q), 135.3 (CH), 130.6 (CH), 126.3 (C_q), 125.6 (CH), 120.0 (CH), 118.8 (CH), 117.0 (CH), 45.7 (CH_3); MS (ESI$^+$): *m/z* (%) = 503.3 (12) [*M* – H]$^+$, 252.3 (100) [*M*]$^{2+}$; purity (LC): 100%; anal. calcd. for $C_{28}H_{24}I_2N_8O_2 \times 2.2\ H_2O$ (798.0): C 42.18, H 3.58, N 14.05; found: C 42.55, H 3.39, N 13.66.

N^{2},*N*^{6}*-Bis[(1-benzylquinolinium-4-yl)methylene]pyridine-2,6-dicarbohydrazide bromide (**PymDH3**):* Yield 93%. Brown crystals. ^{1}H NMR (300 MHz, DMSO-d_6): δ 13.31 (s, 2H), 9.74 (d, *J* = 5.3 Hz, 5H), 8.85 (d, *J* = 8.7 Hz, 2H), 8.74 (s, 1H), 8.60 (dd, *J* = 17.3, 7.6 Hz, 4H), 8.33–8.22 (m, 2H), 8.20–8.12 (m, 2H), 7.40 (s, 10H), 6.42 (s, 4H); ^{13}C NMR (75 MHz, DMSO-d_6): δ 159.7 (C_q), 158.1 (C_q), 157.8 (CH), 149.6 (CH), 147.9 (C_q), 144.3 (CH), 138.2 (C_q), 135.5 (CH), 134.0 (C_q), 130.5 (CH), 129.1 (CH), 128.8 (CH), 127.2 (CH), 127.2 (C_q), 126.1 (CH), 120.1 (CH), 119.2 (CH), 117.1 (CH), 60.0 (CH_2); MS (ESI$^+$): *m/z* (%) = 655.5 (12) [*M* – H]$^+$, 328.4 (100) [*M*]$^{2+}$; purity (LC): 100%; anal. calcd. for $C_{40}H_{32}Br_2N_8O_2 \times H_2O$ (834.6): C 57.57, H 4.11, N 13.43; found: C 57.43, H 4.25, N 13.62.

N^{2},*N*^{6}*-Bis[(1-ethylquinolinium-6-yl)methylene]pyridine-2,6-dicarbohydrazide iodide (**PymDH4**):* Yield 96%. Orange solid. ^{1}H NMR (300 MHz, DMSO-d_6): δ 12.93 (s, 2H), 9.65 (s, 1H), 9.57 (d, *J* = 5.7 Hz, 2H), 9.37 (d, *J* = 8.3 Hz, 2H), 9.00 (s, 2H), 8.80–8.61 (m, 7H), 8.25 (dd, *J* = 8.3, 5.9 Hz, 2H), 5.12 (q, *J* = 7.2 Hz, 4H), 1.64 (t, *J* = 7.2 Hz, 6H); ^{13}C NMR (75 MHz, DMSO-d_6): δ 159.4 (C_q), 158.6 (CH), 149.7 (CH), 148.0 (CH), 147.5 (CH), 138.2 (C_q), 138.1 (C_q), 135.1 (C_q), 132.3 (CH), 130.1 (CH), 130.1 (C_q), 123.2 (CH), 119.9 (CH), 116.8 (CH), 53.2 (CH_2), 15.3 (CH_3); MS (ESI$^+$): *m/z* (%) = 266.3 (100) [*M*]$^{2+}$; purity (LC):

100%; anal. calcd. for $C_{30}H_{28}I_2N_8O_2 \times 3.2\ H_2O$ (844.1): C 42.69, H 4.11, N 13.28; found: C 42.34, H 3.84, N 13.25.

*N'²,N'⁶-Bis[(1-benzylquinolinium-6-yl)methylene]pyridine-2,6-dicarbohydrazide bromide (**PymDH5**):* Yield 97%. Pale-yellow solid. ^{1}H NMR (300 MHz, DMSO-d_6): δ 12.91 (s, 2H), 9.74 (d, J = 5.4 Hz, 2H), 9.62 (d, J = 1.2 Hz, 1H), 9.46 (d, J = 8.3 Hz, 2H), 8.96 (s, 2H), 8.80 (s, 2H), 8.67 – 8.55 (m, 5H), 8.34 (dd, J = 8.3, 5.9 Hz, 2H), 7.47–7.37 (m, 10H), 6.39 (s, 4H); ^{13}C NMR spectrum could not be obtained due to insufficient solubility; MS (ESI$^+$): m/z (%) = 769.5 (7) [M + CF_3COO]$^+$, 328.3 (100) [M]$^{2+}$; purity (LC): 99%; anal. calcd. for $C_{40}H_{32}Br_2N_8O_2 \times 2\ H_2O$ (852.6): C 56.35, H 4.26, N 13.14; found: C 56.09, H 4.20, N 13.21.

*N'²,N'⁷-Bis[(1-methylpyridinium-4-yl)methylene]-1,8-naphthyridine-2,7-dicarbohydrazide iodide (**NaphDH1**):* Yield 76%. Yellow solid; ^{1}H NMR (300 MHz, DMSO-d_6): δ 13.14 (s, 2H), 9.01 (d, J = 6.0 Hz, 4H), 8.94 (d, J = 8.3 Hz, 2H), 8.83 (s, 2H), 8.45 (d, J = 8.3 Hz, 2H), 8.39 (d, J = 5.9 Hz, 4H), 4.36 (s, 6H); ^{13}C NMR (75 MHz, DMSO-d_6): δ 161.6 (C_q), 153.5 (C_q), 152.5 (C_q), 148.9 (C_q), 146.0 (CH), 143.7 (CH), 140.4 (CH), 139.1 (C_q), 124.4 (CH), 122.1 (CH), 47.7 (CH_3); MS (ESI$^+$): m/z (%) = 453.3 (78) [M – H]$^+$, 227.3 (92) [M]$^{2+}$; purity (LC): 100%; anal. calcd. for $C_{24}H_{22}I_2N_8O_2 \times 0.5\ H_2O$ (717.3): C 40.19, H 3.23, N 15.62; found: C 40.29, H 3.47, N 15.56.

*N'²,N'⁷-Bis[(1-methylquinolinium-4-yl)methylene]-1,8-naphthyridine-2,7-dicarbohydrazide iodide (**NaphDH2**):* This compound was obtained in an analytically pure form through a reaction of **3** with **11a** performed in DMSO instead of DMF. Yield 81%. Red solid; ^{1}H NMR (300 MHz, DMSO-d_6): δ 13.14 (s, 2H), 9.72 (s, 2H), 9.52 (d, J = 6.2 Hz, 2H), 8.99 (d, J = 8.3 Hz, 2H), 8.90 (d, J = 8.4 Hz, 2H), 8.68–8.47 (m, 6H), 8.39–8.32 (m, 2H), 8.25–8.15 (m, 2H), 4.67 (s, 6H); ^{13}C NMR spectrum could not be obtained due to insufficient solubility; MS (ESI$^+$): m/z (%) = 553.2 (63) [M – H]$^+$, 277.3 (100) [M]$^{2+}$; purity (LC): 100%; anal. calcd. for $C_{32}H_{26}I_2N_8O_2 \times 0.6$ DMSO (855.3): C 46.62, H 3.49, N 13.10; found: C 46.77, H 3.23, N 13.45.

*N'²,N'⁷-Bis[(1-benzylquinolinium-4-yl)methylene]-1,8-naphthyridine-2,7-dicarbohydrazide bromide (**NaphDH3**):* Yield 90%. Yellow solid; ^{1}H NMR (300 MHz, DMSO-d_6): δ 13.19 (s, 2H), 9.77 (s, 4H), 9.00 (d, J = 8.3 Hz, 2H), 8.90 (d, J = 8.1 Hz, 2H), 8.66 (d, J = 6.0 Hz, 2H), 8.56 (dd, J = 16.8, 8.7 Hz, 4H), 8.32–8.22 (m, 2H), 8.21–8.12 (m, 2H), 7.41 (s, 10H), 6.44 (s, 4H); ^{13}C NMR (75 MHz, DMSO-d_6): δ 161.3 (C_q), 153.2 (C_q), 152.4 (C_q), 149.6 (CH), 148.2 (C_q), 143.1 (CH), 140.6 (CH), 138.2 (C_q), 135.5 (CH), 134.1 (C_q), 130.5 (CH), 129.1 (CH), 128.8 (CH), 127.3 (CH), 127.1 (C_q), 126.1 (CH), 122.0 (CH), 120.2 (CH), 119.0 (CH), 60.0 (CH_2); MS (ESI$^+$): m/z (%) = 705.4 (50) [M – H]$^+$, 353.4 (100) [M]$^{2+}$; purity (LC): 97%; anal. calcd. for $C_{44}H_{34}Br_2N_8O_2 \times 3\ H_2O$ (920.7): C 57.40, H 4.38, N 12.17; found: C 57.28, H 4.21, N 12.11.

N'²,N'⁷-Bis[(1-ethylquinolinium-6-yl)methylene]-1,8-naphthyridine-2,7-dicarbohydrazide iodide (***NaphDH4***)*:* Yield 68%. Pale brown solid; ^{1}H NMR (300 MHz, DMSO-d_6): δ 12.79 (s, 2H), 9.58 (d, J = 5.9 Hz, 2H), 9.38 (d, J = 8.6 Hz, 2H), 8.99 (s, 2H), 8.93 (d, J = 8.4 Hz, 2H), 8.72 (dd, J = 20.4, 11.1 Hz, 6H), 8.45 (d, J = 8.3 Hz, 2H), 8.26 (dd, J = 8.3, 5.8 Hz, 2H), 5.13 (q, J = 7.2 Hz, 4H), 1.65 (t, J = 7.1 Hz, 6H); ^{13}C NMR (75 MHz, DMSO-d_6): δ 161.1 (C_q), 153.8 (C_q), 152.5 (C_q), 149.6 (CH), 148.5 (C_q), 147.4 (CH), 146.8 (CH), 140.3 (CH), 138.0 (C_q), 135.3 (C_q), 132.4 (CH), 130.1 (C_q), 129.9 (CH), 123.2 (CH), 121.8 (CH), 119.9 (CH), 53.3 (CH_2), 15.3 (CH_3); MS (ESI$^+$): m/z (%) = 695.4 (15) [M + CF_3COO]$^+$, 291.3 (100) [M]$^{2+}$; purity (LC): 100%; anal. calcd. for $C_{34}H_{30}I_2N_8O_2$ × 1.5 H_2O (863.5): C 47.29, H 3.85, N 12.98; found: C 47.44, H 4.11, N 12.95.

N'²,N'⁷-Bis[(1-benzylquinolinium-6-yl)methylene]-1,8-naphthyridine-2,7-dicarbohydrazide bromide (***NaphDH5***)*:* Yield 80%. Pale brown solid; ^{1}H NMR (300 MHz, DMSO-d_6): δ 12.76 (s, 2H), 9.75 (d, J = 5.6 Hz, 2H), 9.48 (d, J = 8.3 Hz, 2H), 8.98–8.85 (m, 4H), 8.80 (s, 2H), 8.63 (m, 4H), 8.43 (d, J = 8.3 Hz, 2H), 8.35 (dd, J = 8.2, 5.9 Hz, 2H), 7.41 (d, J = 6.6 Hz, 10H), 6.40 (s, 4H); ^{13}C NMR (75 MHz, DMSO-d_6): δ 161.1 (C_q), 153.8 (C_q), 152.6 (C_q), 150.6 (CH), 148.3 (CH), 146.7 (CH), 140.3 (CH), 138.3 (C_q), 135.5 (C_q), 133.8 (C_q), 132.7 (CH), 130.6 (C_q), 129.8 (CH), 129.2 (C_q), 128.9 (CH), 127.5 (CH), 123.3 (CH), 121.8 (CH), 120.3 (CH), 60.1 (CH_2); MS (ESI$^+$): m/z (%) = 705.4 (5) [M + CF_3COO]$^+$, 353.2 (100) [M]$^{2+}$; purity (LC): 100%; anal. calcd. for $C_{44}H_{34}Br_2N_8O_2$ × H_2O (884.6): C 59.74, H 4.10, N 12.67; found: C 59.55, H 4.44, N 12.56.

N'²,N'⁹-Bis[(1-methylpyridinium-4-yl)methylene]-1,10-phenanthroline-2,9-dicarbohydrazide iodide (***PhenDH1***)*:* Yield 50%. Yellow solid; ^{1}H NMR (300 MHz, DMSO-d_6): δ 13.38 (s, 2H), 9.04 (s, 6H), 8.89 (d, J = 8.1 Hz, 2H), 8.64 (d, J = 8.0 Hz, 2H), 8.41 (d, J = 5.9 Hz, 4H), 8.32 (s, 2H), 4.41 (s, 6H), ^{13}C NMR (75 MHz, DMSO-d_6): δ 161.1 (C_q), 149.3 (C_q), 148.6 (C_q), 146.0 (CH), 144.3 (CH), 143.7 (C_q), 138.9 (CH), 131.1 (C_q), 128.8 (CH), 124.4 (CH), 122.2 (CH), 47.7 (CH_3); MS (ESI$^+$): m/z (%) = 617.3 (20) [M + CF_3COO]$^+$, 503.3 (90) [M – H]$^+$, 252.2 (100%) [M]$^{2+}$; purity (LC): 100%; anal. calcd. for $C_{28}H_{24}I_2N_8O_2$ × 4.6 H_2O (841.2): C 39.98, H 3.98, N 13.32; found: C 40.36, H 4.20, N 12.95.

N'²,N'⁹-Bis[(1-methylquinolinium-4-yl)methylene]-1,10-phenanthroline-2,9-dicarbohydrazide iodide (***PhenDH2***)*:* Yield 78%. Dark-red solid; ^{1}H NMR (300 MHz, DMSO-d_6): δ 13.28 (s, 2H), 9.86 (s, 2H), 9.45 (d, J = 6.3 Hz, 2H), 8.95 (d, J = 8.3 Hz, 2H), 8.71 (d, J = 8.3 Hz, 2H), 8.56 (d, J = 6.1 Hz, 2H), 8.48–8.34 (m, 4H), 8.27 (d, J = 9.1 Hz, 2H), 7.88–7.80 (m, 2H), 7.15–7.08 (m, 2H), 4.62 (s, 6H); ^{13}C NMR (75 MHz, DMSO-d_6): δ 160.6 (C_q), 149.3 (C_q), 148.3 (C_q), 147.3 (C_q), 143.6 (C_q), 143.5 (CH), 139.1 (CH), 138.2 (C_q), 134.6 (CH), 131.2 (C_q), 129.2 (CH), 128.8 (CH), 126.1 (C_q), 125.1 (CH), 122.1 (CH), 119.2 (CH), 118.0 (CH), 45.5 (CH_3); MS (ESI$^+$): m/z (%) = 717.4 (14) [M + CF_3COO]$^+$, 603.4 (83) [M – H]$^+$, 302.3 (100)

[*M*]$^{2+}$; purity (LC): 100%; anal. calcd. for $C_{36}H_{28}I_2N_8O_2$ × 5.7 H_2O (961.2): C 44.99, H 4.13, N 11.66; found: C 45.23, H 4.52, N 11.63.

N'²,N'⁹-Bis[(1-benzylquinolinium-4-yl)methylene]-1,10-phenanthroline-2,9-dicarbohydrazide bromide (***PhenDH3***)*:* Yield 87%. Pale brown solid; ^{1}H NMR (300 MHz, DMSO-d_6): δ 13.34 (s, 2H), 9.94 (s, 2H), 9.76 (d, *J* = 6.0 Hz, 2H), 8.96 (d, *J* = 8.2 Hz, 2H), 8.73 (d, *J* = 7.7 Hz, 4H), 8.37 (d, *J* = 7.9 Hz, 4H), 8.14 (d, *J* = 9.2 Hz, 2H), 7.65–7.30 (m, 10H), 7.09–7.00 (m, 2H), 6.84–6.79 (m, 2H), 6.35 (s, 4H); ^{13}C NMR (75 MHz, DMSO-d_6): δ 160.7 (C_q), 149.6 (CH), 148.4 (C_q), 148.2 (C_q), 143.7 (C_q), 143.2 (CH), 139.1 (CH), 137.5 (C_q), 134.3 (CH), 134.2 (C_q), 131.2 (C_q), 129.2 (CH), 128.9 (CH), 128.8 (CH), 127.3 (C_q), 126.9 (C_q), 125.7 (CH), 122.2 (CH), 119.4 (CH), 118.3 (CH), 118.3 (CH), 59.8 (CH_2); MS (ESI$^+$): *m/z* (%) = 755.4 (20) [*M* – H]$^+$, 378.4 (100) [*M*]$^{2+}$; purity (LC): 100%; anal. calcd. for $C_{48}H_{36}Br_2N_8O_2$ × 3.5 H_2O (979.7): C 58.85, H 4.42, N 11.44; found: C 58.84, H 4.30, N 11.47.

N'²,N'⁹-Bis[(1-ethylquinolinium-6-yl)methylene]-1,10-phenanthroline-2,9-dicarbohydrazide iodide (***PhenDH4***)*:* Yield 72%. Pale brown solid; ^{1}H NMR (300 MHz, DMSO-d_6): δ 13.10 (s, 2H), 9.60 (d, *J* = 5.6 Hz, 2H), 9.25 (s, 2H), 9.17 (d, *J* = 8.2 Hz, 2H), 8.89 (d, *J* = 8.3 Hz, 2H), 8.76 (d, *J* = 2.6 Hz, 6H), 8.64 (d, *J* = 8.3 Hz, 2H), 8.32 (s, 2H), 8.22 (dd, *J* = 8.4, 5.9 Hz, 2H), 5.16 (q, *J* = 7.0 Hz, 4H), 1.67 (t, *J* = 7.1 Hz, 6H); ^{13}C NMR (75 MHz, DMSO-d_6): δ 160.7 (C_q), 149.6 (CH), 149.0 (C_q), 147.3 (C_q), 147.2 (CH), 143.7 (C_q), 138.7(CH), 138.0 (C_q), 135.7 (C_q), 132.8 (CH), 130.9 (C_q), 130.1 (C_q), 129.3 (CH), 128.5 (CH), 123.2 (CH), 122.0 (CH), 120.0 (CH), 53.3 (CH_2), 15.4 (CH_3); MS (ESI$^+$): *m/z* (%) = 745.4 (28) [*M* + CF_3COO]$^+$, 316.2 (100) [*M*]$^{2+}$; purity (LC): 98%; anal. calcd. for $C_{38}H_{32}I_2N_8O_2$ × 1.5 H_2O (904.5): C 50.46, H 3.79, N 12.39; found: C 50.13, H 3.90, N 12.41.

N'²,N'⁹-Bis[(1-benzylquinolinium-6-yl)methylene]-1,10-phenanthroline-2,9-dicarbohydrazide bromide (***PhenDH5***)*:* Yield 91%. Pale brown solid; ^{1}H NMR (300 MHz, DMSO-d_6): δ 13.10 (s, 2H), 9.79 (d, *J* = 5.7 Hz, 2H), 9.30 (d, *J* = 8.3 Hz, 2H), 9.21 (s, 2H), 8.87 (d, *J* = 8.3 Hz, 2H), 8.81 (s, 2H), 8.76–8.65 (m, 4H), 8.63 (d, *J* = 8.3 Hz, 2H), 8.39–8.28 (m, 4H), 7.53–7.37 (m, 10H), 6.46 (s, 4H); ^{13}C NMR (75 MHz, DMSO-d_6): δ 160.7 (C_q), 150.5 (CH), 149.0 (C_q), 148.1 (CH), 147.0 (CH), 143.8 (C_q), 138.7 (CH), 138.3 (C_q), 135.9 (C_q), 133.8 (C_q), 133.0 (CH), 130.9 (C_q), 130.4 (C_q), 129.5 (CH), 129.2 (CH), 128.9 (CH), 128.6 (CH), 127.6 (CH), 123.4 (CH), 122.0 (CH), 120.3 (CH), 60.1 (CH_2); MS (ESI$^+$): *m/z* (%) = 755.4 (5) [*M* – H]$^+$, 378.4 (100) [*M*]$^{2+}$; purity (LC): 100%; anal. calcd. for $C_{48}H_{36}Br_2N_8O_2$ × 2 H_2O (952.7): C 60.51, H 4.23, N 11.76; found: C 60.76, H 4.39, N 11.77.

5.2. Single-crystal X-ray diffraction analysis

X-ray diffraction data for **PyDH1** ($2I^-$) were collected using a VENTURE PHOTON100 CMOS Bruker diffractometer with Micro-focus IuS source Mo $_{K\alpha}$ radiation. X-ray diffraction data for **PymDH1** ($2I^-$) were collected using a X8 APEXII CCD Bruker diffractometer with graphite-monochromated Mo $_{K\alpha}$

radiation. X-ray diffraction data for **PhenDH1** ($2I^-$) were collected using a VENTURE PHOTON100 CMOS Bruker diffractometer with Micro-focus IuS source Cu $_{K\alpha}$ radiation. All crystals were mounted on a CryoLoop (Hampton Research) with Paratone-N (Hampton Research) as cryoprotectant and then flash-frozen in a nitrogen gas stream at 100 K. For compounds, the temperature of the crystal was maintained at the selected value by means of a 700 series Cryostream (for X8) or N-Helix (for VENTURE) cooling device within an accuracy of ±1 K. The data were corrected for Lorentz polarization, and absorption effects. The structures were solved by direct methods using SHELXS-97 [48] and refined against F^2 by full-matrix least-squares techniques using SHELXL-2018 [49] with anisotropic displacement parameters for all non-hydrogen atoms. All calculations were performed using the Crystal Structure crystallographic software package WINGX [50]. The crystal data collection and refinement parameters are given in Table S3. CCDC 1881844–1881846 contain the supplementary crystallographic data for this paper. These data can be obtained free of charge from the Cambridge Crystallographic Data Centre via https://www.ccdc.cam.ac.uk/structures/.

5.3. Biophysical assays

5.3.1. Fluorescence melting assay

The assay was performed with a double-labeled oligoribonucleotide (g4-EBNA1, 5'-FAM-r(GGGGCAGGAGCAGGAGGA)-TAMRA-3'), which was annealed prior to experiments (95 °C, 5 min) in K-10 buffer (10 mM $LiAsO_2Me_2$, 10 mM KCl, 90 mM LiCl, pH 7.3) at a concentration of 10 µM. Double-stranded DNA competitor (ds26, 5'-CAATCGGATCGAATTCGATCCGATTG-3') was annealed in the same buffer at a strand concentration of 200 µM. Thermal denaturation runs were performed in 96-well plates with a real-time PCR apparatus (7900HT Fast Real-Time PCR, Applied Biosystems) using a heating ramp of 0.5 °C per minute from 25 to 95 °C; the fluorescence intensity was monitored in the FAM channel. Each well contained 0.2 µM of double-labeled g4-EBNA1, 1 µM of tested compound, and/or 0, 3 or 10 µM of ds26 competitor, in a total volume of 25 µL of K10 buffer. The denaturation temperatures (T_m) were determined from the maxima of first-derivative plots of FAM emission intensity vs. temperature, and ligand-induced T_m shifts (ΔT_m) were calculated as a difference of mean denaturation temperatures in the presence and in the absence of ligands (T_m^0 = 58.6 °C), from three independent experiments. Analogous experiments were performed with G4-forming DNA oligonucleotides F-myc22-T: 5'-FAM-d(TGAGGGTGGGTAGGGTGGGTAA)-TAMRA-3' and F-25TAG-T: 5'-FAM-d(TAGGGTTAGGGTTAGGGTTAGGGAA)-TAMRA-3', in K-1 (10 mM $LiAsO_2Me_2$, 1 mM KCl, 99 mM LiCl, pH 7.3) and K-100 (10 mM $LiAsO_2Me_2$, 100 mM KCl, pH 7.3) buffers, respectively.

5.3.2. TO displacement assay

This assay is performed in a 96-well microplate format as described [39]. The non-labeled g4-EBNA1 oligoribonucleotide was annealed (95 °C, 5 min) in K100 buffer (10 mM $KAsO_2Me_2$, 100 mM KCl, 1 mM EDTA, 1% v/v DMSO) at a concentration of 5 µM and, after cooling, supplemented with TO (10 µM). Every row of a black-bottom, 96-well microplate was filled with K100 buffer (q.s.p. 200 µL per well), pre-folded g4-EBNA1 + TO solution (final concentrations: 0.25 and 0.5 µM, respectively), and an extemporaneously prepared ligand solution (5 µM in the same buffer; final ligand concentration: 0 to 2.5 µM). After 5 min of orbital shaking, fluorescence intensity was measured with a Fluostar Omega microplate reader (BMG Labtech) using the following parameters: 20 flashes per well, emission / excitation filters: 485 / 520 nm, gain adjusted at 80% of the fluorescence from the most fluorescent well. The experiments were performed in duplicate. The percentage of TO displacement was calculated from the fluorescence intensity (F) as %(TO displacement) = $100 \times (1 - F / F_0)$, where F_0 is the fluorescence intensity of TO–RNA complex in the absence of ligands. The percentage of displacement was plotted against the concentration of added ligand, and ligand affinity was characterized by the concentration required to decrease the fluorescence of the probe by 50% (DC_{50}) after interpolation of the displacement curve. A control experiment was performed at identical conditions with double-stranded DNA substrate ds26.

5.4. Biological assays

5.4.1. EBNA1 expression assay

The human lung carcinoma cell line H1299 was cultured in RPMI-1640 medium supplemented with 10% fetal bovine serum (FBS), 2 mM L-glutamine, 100 U mL^{-1} penicillin, and 100 µg mL^{-1} streptomycin. All cells were cultured at 37 °C with 5% CO_2. Transient transfections were performed using Genejuice reagent (Merck Bioscience) according to the manufacturer's protocol. For cell treatments with the indicated G4 ligands or **PhenDC3**, cells were incubated with 10 µM of drug for 40 h after transfection. Stock solutions of drugs were prepared in DMSO (Euromedex). Whole-cell lysates were prepared 48 h post-transfection, and protein concentration was determined using a Bradford assay. Samples were electrophoretically separated in NuPAGE® Bis-Tris gels 10% (Invitrogen), transferred onto 0.45 µm nitrocellulose membranes (GE) and blotted under standard conditions using the following antibodies: anti-GAPDH (Sigma, 1:5,000), anti-EBNA1 mouse monoclonal antibody (OT1X, 1:2,000) or anti-OVA rabbit polyclonal antibody (C6534 Sigma, 1:2,500). The membranes were then washed with fresh PBS, 1X 0.1% Igepal and incubated for 45 min with swine anti-rabbit or goat anti-mouse secondary antibodies (Dako) conjugated to horseradish peroxidase at a 1:3,000 dilution, and analyzed by enhanced chemiluminescence (ECL, GE Healthcare) using a Chemistart 5000 imager (Vilber–Lourmat). All experiments were repeated at least three

times. Relative protein levels for each sample were normalized to GAPDH or Actin levels as indicated, using Fusion-Capt Advance software.

5.4.2. Antigen presentation assay

Naive $OVA_{257–264}$ specific $CD8^+$ T cells were isolated by negative selection from peripheral and mesenteric lymph nodes of a 12-week-old female OT-I mice using the $CD8^+$ T cell isolation kit (Miltenyi Biotec, Germany). Afterwards, $CD8^+$ T cells were co-cultured with H1299 cells co-transfected with mouse Kb expression vector and the indicated constructs. For all assays, 10^5 H1299 cells were harvested 40 h after treatment and co-incubated with 4×10^5 $CD8^+$ T cells at 37 °C in humidified air/CO_2 atmosphere in RPMI medium containing 10% FBS, 4 mM L-glutamine, 100 U mL^{-1} penicillin, 100 µg mL^{-1} streptomycin, 5 mM HEPES and 0.05 mM 2-mercaptoethanol. After 3 days of co-incubation, supernatants were collected and IL-2 levels were measured employing the IL-2 ELISA MAX™ Standard kit (Biolegend, USA) according to the manufacturer's instructions.

5.4.3. MTT toxicity assay

About 30,000 Mutu-1 cells (derived from an EBV-positive Burkitt's lymphoma biopsy specimen from a Kenyan patient) were plated in 0.1 mL per well in 96-well, flat-bottom plates and exposed to the indicated compounds at the indicated concentrations or DMSO (vehicle). After indicated time (24 or 48 h), 10 µL of MTT solution (5 mg mL^{-1}, CT01-5, Merck Millipore) in PBS (pH 7.4) was added to each well and incubated for 4 h. A mixture of isopropanol / 0.1 N HCl / 10% Triton X-100 (0.1 mL) was added to each well to dissolve the formazan crystals, and the absorbance was then measured at 540 nm.

5.4.4. PLA assay

H1299 cells were transfected with an EBNA1 construct and, 7 h post-transfection, treated with the tested compounds during 40 h. In the experiments with Mutu-1 cells expressing endogenous EBNA1 mRNA, drug treatment was carried out during 36 h. Following compounds administration, cells were processed as previously described [42]. Briefly, paraformaldehyde-fixed samples were incubated in 70% (v/v) ethanol at 4 °C overnight, rehydrated in PBS for 30 min, and permeabilized in PBS 0.4% Triton X-100, 0.05% CHAPS for 10 min at room temperature. Before the *in situ* hybridization step, samples were pre-treated with hybridization buffer (10% formamide, 2X SSC buffer, 0.2 mg mL^{-1} *E. coli* 522 tRNAs, 0.2 mg mL^{-1} sheared salmon sperm DNA, and 2 mg mL^{-1} BSA) and then incubated overnight with 50 ng of an EBNA1-digoxigenin DNA probe (5'-CTTTCCAAACCACCCTCCTTTTTTGCGCCT-GCCTCCATCAAAAA-digoxigenin-3') in a humidified chamber at 37 °C. To avoid secondary structure formation, the probe was diluted in 5 µL of water, denatured at 80 °C for 5 min, chilled on ice for 5 min, and then re-suspended in 35 µL of hybridization buffer. After hybridization, samples were

serially washed for 20 min with 2X SSC buffer, 10% formamide, hybridization buffer (twice), 2X SSC buffer, and PBS. Samples were then saturated with PBS 3% BSA for 30 min and incubated for 2 h at room temperature with a mix of primary antibodies containing the mouse anti-digoxigenin (clone DI-22, Sigma, 1:200) and the rabbit anti-nucleolin (ab22758, Abcam, 1:1,000). Subsequently, PLA was carried out using the anti-rabbit plus and anti-mouse minus Duolink probes (Sigma) and the Duolink FarRed PLA *in situ* kit (Sigma) following the manufacturer's protocol. Experiments were performed in duplicate and 100 cells per sample and per replicate were imaged and analyzed.

5.4.5. RNA pull-down assay

These experiments were performed as previously described [22,51]. Briefly, recombinant NCL (kind ly provided by Prof. Weinhold, Aachen, Germany) was used for pulldown assays with the following RNA oligonucleotides: g4-EBNA1 (5'-GGGGCAGGAGCAGGAGGA-3'-TEG-Biotin) or GM (5'-GAGGCAGUAG-CAGUAGAA-3'-TEG-Biotin, not able to form G4 according to the GQRS-H software). To allow the formation of the G4, the oligonucleotides were resuspended in the folding buffer (10 mM Tris-HCl pH 7.5, 100 mM KCl, 0.1 mM EDTA;), heated at 95 °C for 5 min, and then slowly and progressively cooled down to 4 °C (cooling rate of 2 °C min^{-1}) using a Veriti thermal cycler (Applied BioSsystems). To avoid unspecific binding, high-affinity streptavidin sepharose beads (GE Healthcare) were incubated in 1 mL blocking buffer containing (10 mM Tris-HCl pH 7.5, 100 mM KCl, 0.1 mM EDTA, 1 mM DTT, 0.01% Triton X-100, 0.1% BSA, 0.02% *S. cerevisiae* tRNAs) for 1 h at 4 °C on a rotating wheel. A 10-pg amount of folded biotinylated RNA oligonucleotide was incubated with 50 µL of suspension containing the streptavidin-coupled sepharose beads for 90 min at 4 °C on a rotating wheel. Then, 200 ng of recombinant NCL was incubated with the RNA oligonucleotides bound to the beads during 90 min at room temperature. Beads were washed with increasing KCl concentration (200 to 800 mM). Protein still bound to beads after the washes were eluted using 2X SDS loading buffer and analyzed by western blotting against NCL, as previously described. In the input lane of the western blots was loaded a quantity of recombinant NCL protein which corresponds to half of the quantity that was incubated with the beads for each condition.

ACKNOWLEDGMENTS

We thank Ms. Anne Cucchiarini for help with chromatographic analyses and Ms. Patricia Duchambon (Institut Curie) for the NCL plasmid construct. This work was supported by *Agence Nationale de Recherche* (grant-in aid ANR-17-CE07-0004-01 to AG), French Ministry of Higher Education, Research and Innovation (PhD fellowship for OR), *La Ligue contre le Cancer* (to RF), *La Ligue contre le Cancer – CSIRGO* (grant 2017-18 to MB), *Institut National du Cancer* (grant 2016-169 to MB, RF, and MPTF), and *Fondation pour la Recherche Médicale* (grant DCM20181039571 to MB, RF, and MPTF). JGG

thanks the Department of Education, Research and Sport of the Valencian Community for a postdoctoral VALi+d fellowship.

ABBREVIATIONS

BOILED, Brain Or IntestinaL EstimateD permeation; EBNA1, EBV-encoded nuclear antigen-1; EBV, Epstein–Barr virus; FID, fluorescent indicator displacement; G4, G-quadruplex; GAr, glycine–alanine repeat; IL-2, Interleukin-2; MHC, major histocompatibility complex; OVA, ovalbumin; PLA, proximity ligation assay; TO, Thiazole Orange.

SUPPLEMENTARY DATA

Supplementary data to this article can be found online.

DECLARATION OF INTERESTS

None.

REFERENCES

[1] M.P. Thompson, R. Kurzrock, Epstein-Barr Virus and Cancer, Clin. Cancer Res. 10 (2004) 803–821. doi:10.1158/1078-0432.CCR-0670-3.

[2] J.L. Hsu, S.L. Glaser, Epstein–Barr virus-associated malignancies: epidemiologic patterns and etiologic implications, Crit. Rev. Oncol. Hematol. 34 (2000) 27–53. doi:10.1016/S1040-8428(00)00046-9.

[3] J. Levitskaya, M. Coram, V. Levitsky, S. Imreh, P.M. Steigerwald-Mullen, G. Klein, M.G. Kurilla, M.G. Masucci, Inhibition of antigen processing by the internal repeat region of the Epstein–Barr virus nuclear antigen-1, Nature. 375 (1995) 685–688. doi:10.1038/375685a0.

[4] Y. Yin, B. Manoury, R. Fåhraeus, Self-Inhibition of Synthesis and Antigen Presentation by Epstein-Barr Virus-Encoded EBNA1, Science. 301 (2003) 1371–1374. doi:10.1126/science.1088902.

[5] J. Wilson, E. Manet, H. Gruffat, P. Busson, M. Blondel, R. Fahraeus, EBNA1: Oncogenic Activity, Immune Evasion and Biochemical Functions Provide Targets for Novel Therapeutic Strategies against Epstein–Barr Virus-Associated Cancers, Cancers. 10 (2018) 109. doi:10.3390/cancers10040109.

[6] J. Tellam, G. Connolly, K.J. Green, J.J. Miles, D.J. Moss, S.R. Burrows, R. Khanna, Endogenous Presentation of CD8 + T Cell Epitopes from Epstein-Barr Virus–encoded Nuclear Antigen 1, J.

Exp. Med. 199 (2004) 1421–1431. doi:10.1084/jem.20040191.

[7] P. Murat, J. Zhong, L. Lekieffre, N.P. Cowieson, J.L. Clancy, T. Preiss, S. Balasubramanian, R. Khanna, J. Tellam, G-quadruplexes regulate Epstein-Barr virus-encoded nuclear antigen 1 mRNA translation., Nat. Chem. Biol. 10 (2014) 358–64. doi:10.1038/nchembio.1479.

[8] H.J. Lipps, D. Rhodes, G-quadruplex structures: in vivo evidence and function, Trends Cell Biol. 19 (2009) 414–422. doi:10.1016/j.tcb.2009.05.002.

[9] T. Tian, Y.Q. Chen, S.R. Wang, X. Zhou, G-Quadruplex: A Regulator of Gene Expression and Its Chemical Targeting, Chem. 4 (2018) 1314–1344. doi:10.1016/j.chempr.2018.02.014.

[10] D. Rhodes, H.J. Lipps, G-quadruplexes and their regulatory roles in biology, Nucleic Acids Res. 43 (2015) 8627–8637. doi:10.1093/nar/gkv862.

[11] M.M. Fay, S.M. Lyons, P. Ivanov, RNA G-Quadruplexes in Biology: Principles and Molecular Mechanisms, J. Mol. Biol. 429 (2017) 2127–2147. doi:10.1016/j.jmb.2017.05.017.

[12] M. Metifiot, S. Amrane, S. Litvak, M.-L. Andreola, G-quadruplexes in viruses: function and potential therapeutic applications, Nucleic Acids Res. 42 (2014) 12352–12366. doi:10.1093/nar/gku999.

[13] L.M. Harris, C.J. Merrick, G-Quadruplexes in Pathogens: A Common Route to Virulence Control?, PLOS Pathog. 11 (2015) e1004562. doi:10.1371/journal.ppat.1004562.

[14] A. Cammas, S. Millevoi, RNA G-quadruplexes: emerging mechanisms in disease, Nucleic Acids Res. 45 (2017) 1584–1595. doi:10.1093/nar/gkw1280.

[15] E. Ruggiero, S.N. Richter, G-quadruplexes and G-quadruplex ligands: targets and tools in antiviral therapy, Nucleic Acids Res. 46 (2018) 3270–3283. doi:10.1093/nar/gky187.

[16] S. Seifert, Above and Beyond Watson and Crick: Guanine Quadruplex Structures and Microbes, Annu. Rev. Microbiol. 72 (2018) 49–69. doi:10.1146/annurev-micro-090817.

[17] S. Pandey, P. Agarwala, S. Maiti, Targeting RNA G-Quadruplexes for Potential Therapeutic Applications, in: Top. Med. Chem., 2017: pp. 177–206. doi:10.1007/7355_2016_22.

[18] C. Voisset, C. Daskalogianni, M.-A. Contesse, A. Mazars, H. Arbach, M. Le Cann, F. Soubigou, S. Apcher, R. Fåhraeus, M. Blondel, A yeast-based assay identifies drugs that interfere with immune evasion of the Epstein–Barr virus, Dis. Model. Mech. 7 (2014) 435–444. doi:10.1242/dmm.014308.

[19] M.J. Lista, C. Voisset, M.A. Contesse, G. Friocourt, C. Daskalogianni, F. Bihel, R. Fåhraeus, M. Blondel, The long-lasting love affair between the budding yeast Saccharomyces cerevisiae and the Epstein-Barr virus, Biotechnol. J. 10 (2015) 1670–1681. doi:10.1002/biot.201500161.

[20] M.J. Lista, R.P. Martins, G. Angrand, A. Quillévéré, C. Daskalogianni, C. Voisset, M.-P. Teulade-Fichou, R. Fåhraeus, M. Blondel, A yeast model for the mechanism of the Epstein-Barr virus immune evasion identifies a new therapeutic target to interfere with the virus stealthiness, Microb. Cell. 4 (2017) 305–307. doi:10.15698/mic2017.09.590.

[21] K. Abdelmohsen, M. Gorospe, RNA-binding protein nucleolin in disease, RNA Biol. 9 (2012) 799–808. doi:10.4161/rna.19718.

[22] M.J. Lista, R.P. Martins, O. Billant, M.-A. Contesse, S. Findakly, P. Pochard, C. Daskalogianni, C. Beauvineau, C. Guetta, C. Jamin, M.-P. Teulade-Fichou, R. Fåhraeus, C. Voisset, M. Blondel, Nucleolin directly mediates Epstein–Barr virus immune evasion through binding to G-quadruplexes of EBNA1 mRNA, Nat. Commun. 8 (2017) 16043. doi:10.1038/ncomms16043.

[23] W.J. Chung, B. Heddi, F. Hamon, M.-P. Teulade-Fichou, A.T. Phan, Solution Structure of a G-quadruplex Bound to the Bisquinolinium Compound Phen-DC 3, Angew. Chem. Int. Ed. 53 (2014) 999–1002. doi:10.1002/anie.201308063.

[24] S. Thota, D.A. Rodrigues, P. de S.M. Pinheiro, L.M. Lima, C.A.M. Fraga, E.J. Barreiro, N-Acylhydrazones as drugs, Bioorg. Med. Chem. Lett. 28 (2018) 2797–2806. doi:10.1016/j.bmcl.2018.07.015.

[25] C. Fraga, E. Barreiro, Medicinal Chemistry of N-Acylhydrazones: New Lead-Compounds of Analgesic, Antiinflammatory and Antithrombotic Drugs, Curr. Med. Chem. 13 (2006) 167–198. doi:10.2174/092986706775197881.

[26] J. Tributino, M. Santos, C. Mesquita, C. Lima, L. Silva, R. Maia, C. Duarte, E. Barreiro, C. Fraga, N. Castro, A. Miranda, M. Guimaraes, LASSBio-881: An N-acylhydrazone transient receptor potential vanilloid subfamily type 1 antagonist orally effective against the hypernociception induced by capsaicin or partial sciatic ligation, Br. J. Pharmacol. 159 (2010) 1716–1723. doi:10.1111/j.1476-5381.2010.00672.x.

[27] D.A. Rodrigues, G.A. Ferreira-Silva, A.C.S. Ferreira, R.A. Fernandes, J.K. Kwee, C.M.R. SantAnna, M. Ionta, C.A.M. Fraga, Design, Synthesis, and Pharmacological Evaluation of Novel N-Acylhydrazone Derivatives as Potent Histone Deacetylase 6/8 Dual Inhibitors, J. Med. Chem. 59 (2016) 655–670. doi:10.1021/acs.jmedchem.5b01525.

[28] S. Rollas, S. Küçükgüzel, Biological Activities of Hydrazone Derivatives, Molecules. 12 (2007) 1910–1939. doi:10.3390/12081910.

[29] R. do C. Maia, R. Tesch, C.A.M. Fraga, Acylhydrazone derivatives: a patent review, Expert Opin. Ther. Pat. 24 (2014) 1161–1170. doi:10.1517/13543776.2014.959491.

[30] M. Alam, G. Verma, M. Shaquiquzzaman, A. Marella, M. Akhtar, M. Ali, A review exploring biological activities of hydrazones, J. Pharm. Bioallied Sci. 6 (2014) 69. doi:10.4103/0975-7406.129170.

[31] A. Emission, K. Santhiya, S.K. Sen, R. Natarajan, R. Shankar, D–A–D Structured Bis-acylhydrazone Exhibiting Aggregation-Induced Emission, Mechanochromic Luminescence, and Al(III) Detection, J. Org. Chem. 83 (2018) 10770–10775. doi:10.1021/acs.joc.8b01377.

[32] A. Daina, O. Michielin, V. Zoete, SwissADME: A free web tool to evaluate pharmacokinetics, drug-likeness and medicinal chemistry friendliness of small molecules, Sci. Rep. 7 (2017) 1–13. doi:10.1038/srep42717.

[33] I. Muegge, S.L. Heald, D. Brittelli, Simple Selection Criteria for Drug-like Chemical Matter, J. Med. Chem. 44 (2001) 1841–1846. doi:10.1021/jm015507e.

[34] A. Daina, V. Zoete, A BOILED-Egg To Predict Gastrointestinal Absorption and Brain Penetration of Small Molecules, ChemMedChem. (2016) 1117–1121. doi:10.1002/cmdc.201600182.

[35] J.B. Baell, G.A. Holloway, New Substructure Filters for Removal of Pan Assay Interference Compounds (PAINS) from Screening Libraries and for Their Exclusion in Bioassays, J. Med. Chem. 53 (2010) 2719–2740. doi:10.1021/jm901137j.

[36] A. De Cian, L. Guittat, M. Kaiser, B. Saccà, S. Amrane, A. Bourdoncle, P. Alberti, M.-P. Teulade-Fichou, L. Lacroix, J.-L. Mergny, Fluorescence-based melting assays for studying quadruplex ligands., Methods. 42 (2007) 183–195. doi:10.1016/j.ymeth.2006.10.004.

[37] A.T. Phan, V. Kuryavyi, K.N. Luu, D.J. Patel, Structure of two intramolecular G-quadruplexes formed by natural human telomere sequences in K+ solution, Nucleic Acids Res. 35 (2007) 6517–6525. doi:10.1093/nar/gkm706.

[38] H.T. Le, M.C. Miller, R. Buscaglia, W.L. Dean, P. a Holt, J.B. Chaires, J.O. Trent, Not all G-quadruplexes are created equally: an investigation of the structural polymorphism of the c-Myc G-quadruplex-forming sequence and its interaction with the porphyrin TMPyP4., Org. Biomol. Chem. 10 (2012) 9393–404. doi:10.1039/c2ob26504d.

[39] E. Largy, F. Hamon, M.-P. Teulade-Fichou, Development of a high-throughput G4-FID assay for screening and evaluation of small molecules binding quadruplex nucleic acid structures., Anal. Bioanal. Chem. 400 (2011) 3419–27. doi:10.1007/s00216-011-5018-z.

[40] I. Weibrecht, K.-J. Leuchowius, C.-M. Clausson, T. Conze, M. Jarvius, W.M. Howell, M. Kamali-Moghaddam, O. Söderberg, Proximity ligation assays: a recent addition to the proteomics toolbox, Expert Rev. Proteomics. 7 (2010) 401–409. doi:10.1586/epr.10.10.

[41] D. Gomez, L.S. Shankman, A.T. Nguyen, G.K. Owens, Detection of histone modifications at specific gene loci in single cells in histological sections, Nat. Methods. 10 (2013) 171–177. doi:10.1038/nmeth.2332.

[42] R. Prado Martins, S. Findakly, C. Daskalogianni, M.-P. Teulade-Fichou, M. Blondel, R. Fåhraeus, R. Prado Martins, S. Findakly, C. Daskalogianni, M.-P. Teulade-Fichou, M. Blondel, R. Fåhraeus, In Cellulo Protein-mRNA Interaction Assay to Determine the Action of G-Quadruplex-Binding Molecules, Molecules. 23 (2018) 3124. doi:10.3390/molecules23123124.

[43] V. Dhamodharan, S. Harikrishna, C. Jagadeeswaran, K. Halder, P.I. Pradeepkumar, Selective G-quadruplex DNA Stabilizing Agents Based on Bisquinolinium and Bispyridinium Derivatives of 1,8-Naphthyridine, J. Org. Chem. 77 (2012) 229–242. doi:10.1021/jo201816g.

[44] V. Dhamodharan, S. Harikrishna, A.C. Bhasikuttan, P.I. Pradeepkumar, Topology Specific Stabilization of Promoter over Telomeric G-Quadruplex DNAs by Bisbenzimidazole Carboxamide Derivatives, ACS Chem. Biol. 10 (2015) 821–833. doi:10.1021/cb5008597.

[45] R.M. Duke, J.E. O'Brien, T. McCabe, T. Gunnlaugsson, Colorimetric sensing of anions in aqueous solution using a charge neutral, cleft-like, amidothiourea receptor: tilting the balance between hydrogen bonding and deprotonation in anion recognition, Org. Biomol. Chem. 6 (2008) 4089. doi:10.1039/b807579d.

[46] R.A. Evangelista, A. Pollak, E.F. Gudgin Templeton, Enzyme-amplified lanthanide luminescence for enzyme detection in bioanalytical assays, Anal. Biochem. 197 (1991) 213–224. doi:10.1016/0003-2697(91)90381-3.

[47] S. Barman, K.L. Diehl, E. V. Anslyn, The effect of alkylation, protonation, and hydroxyl group substitution on reversible alcohol and water addition to 2- and 4-formyl pyridine derivatives, RSC Adv. 4 (2014) 28893–28900. doi:10.1039/c4ra03466j.

[48] G.M. Sheldrick, SHELXS-97, program for X-ray crystal structure solution, University of Gottingen, Germany, 1997.

[49] G.M. Sheldrick, Crystal structure refinement with SHELXL, Acta Crystallogr. Sect. C Struct. Chem. 71 (2015) 3–8. doi:10.1107/S2053229614024218.

[50] L.J. Farrugia, WinGX suite for small-molecule single-crystal crystallography, J. Appl. Crystallogr. 32 (1999) 837–838. doi:10.1107/S0021889899006020.

[51] A. von Hacht, O. Seifert, M. Menger, T. Schütze, A. Arora, Z. Konthur, P. Neubauer, A. Wagner, C. Weise, J. Kurreck, Identification and characterization of RNA guanine-quadruplex binding proteins, Nucleic Acids Res. 42 (2014) 6630–6644. doi:10.1093/nar/gku290.